Metal–Organic Frameworks

DOI: 10.1002/anie.201002451

Surface Chemistry of Metal–Organic Frameworks at the Liquid–Solid Interface

*Denise Zacher, Rochus Schmid, Christof Wöll, and Roland A. Fischer**

Keywords:
coordination modulation · heterostructures · layer-by-layer growth · metal-organic framework · surface chemistry

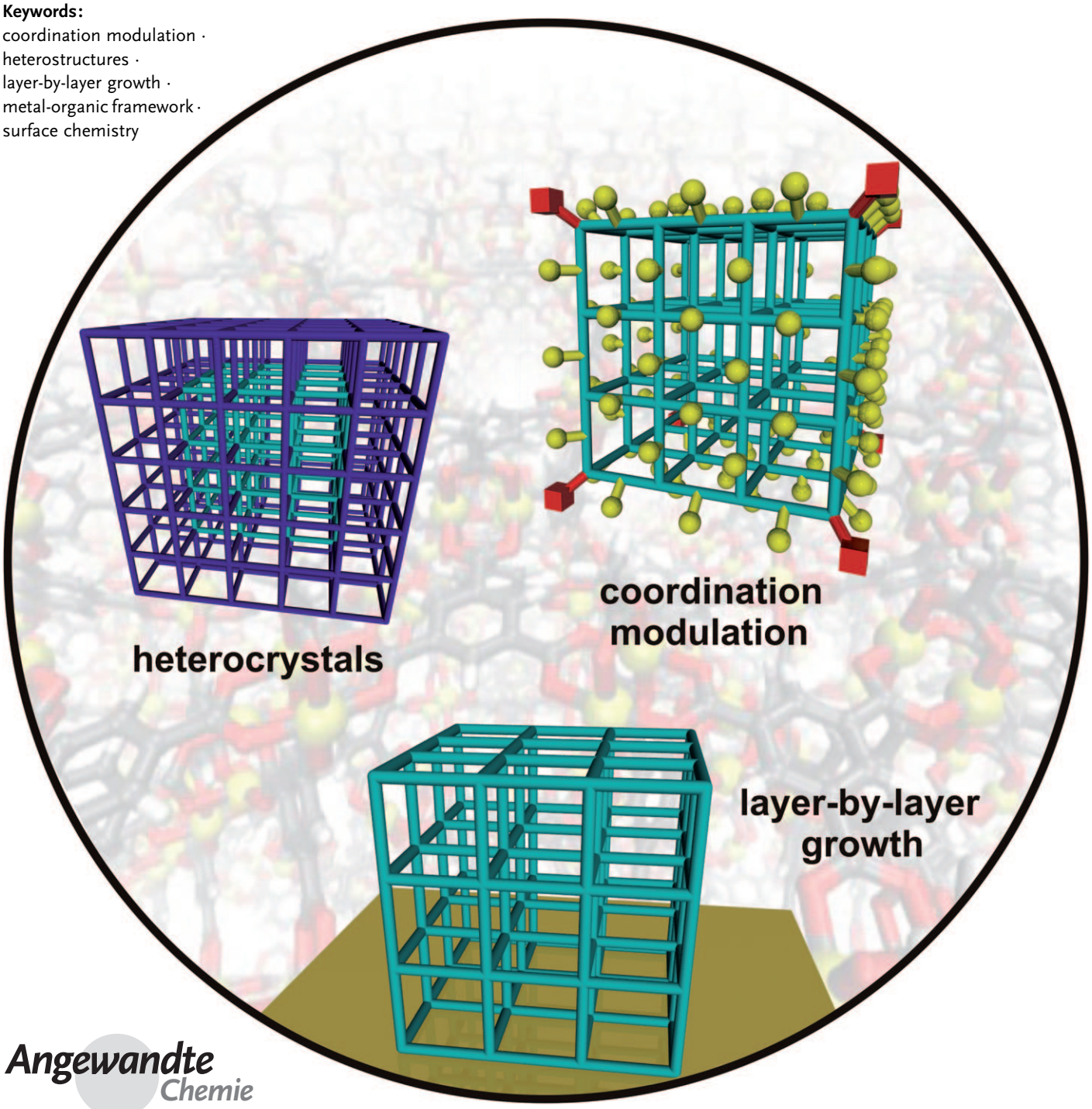

Metal–organic frameworks (MOFs) are a fascinating class of novel inorganic–organic hybrid materials. They are essentially based on classic coordination chemistry and hold much promise for unique applications ranging from gas storage and separation to chemical sensing, catalysis, and drug release. The evolution of the full innovative potential of MOFs, in particular for nanotechnology and device integration, however requires a fundamental understanding of the formation process of MOFs. Also necessary is the ability to control the growth of thin MOF films and the positioning of size- and shape-selected crystals as well as MOF heterostructures on a given surface in a well-defined and oriented fashion. MOFs are solid-state materials typically formed by solvothermal reactions and their crystallization from the liquid phase involves the surface chemistry of their building blocks. This Review brings together various key aspects of the surface chemistry of MOFs.

From the Contents

1. Introduction

Crystalline porous coordination polymers (PCPs), also called metal–organic frameworks (MOFs), are a fascinating class of solid-state inorganic–organic hybrid materials. Research into these compounds is expanding very rapidly owing to their exciting combination of properties for advanced functional materials in gas storage and gas separation, catalysis, chemical sensing, as well as medical applications.[1–6] A leading idea of this largely Werner-type coordination chemistry is the (formal) persistence of the structural integrity of the individual building blocks during the assembly process. These units are metal complexes or oligonuclear metal ion clusters (also called secondary building units, SBUs, similar to zeolite chemistry) and di- or oligotopic organic linkers, being more spacious and chemically more diverse than simple, small inorganic ambidentate ions (e.g. cyanide), and may be maintained throughout the reactions (including post synthesis functionalization). These units join together and form comparably strong ionic and/or donor–acceptor bonds. This coordination chemistry combined with the topological and steric/conformational properties of the individual units allows the development of a rational concept of reticular synthesis.

The principles of the so-called reticular synthesis of PCPs and MOFs, their chemical and physical properties based on permanent porosity including reversible host–guest interactions as well as the numerous perspectives for applications, have been reviewed extensively over the last few years.[1–8] There is some concern about exact definitions and reasonable distinctions between PCPs and MOFs, including the debate on rational synthesis, design, and predictability. Interesting arguments have been put forward by leading authors in the field.[7] For the purpose of this Review, however, these distinctions are not particularly relevant and the acronym MOF will be used with the understanding that PCPs are included (and all other coordination polymers that are not chemically robust, and are without permanent porosity and reversible host–guest chemistry are excluded).

Most of the research on the properties and applications of MOFs deal with microcrystalline powder samples. Much progress has been made towards the control of size, shape distribution, and modulation of the pores, as well as the tailoring of the internal coordination space provided by these materials. Nevertheless, almost nothing is known on the mechanistic details and kinetics of MOF formation under the typical conditions of solvothermal synthesis.[8] This lack of data has consequences for the important area of future development in MOF materials chemistry, namely, MOF surface chemistry at the liquid–solid interface. This area includes the materials chemistry of MOF thin films and MOF nanoparticles. Both fields are far less developed in comparison to the over-all very rapid progress in MOF research. As MOFs are essentially solid-state materials and insoluble in any solvent without decomposition, it is not at all straight forward to deposit MOF materials as homogeneous films and/or ultrathin well-defined crystalline layers on a given substrate for subsequent integration into any functional devices, such as chemical sensors and smart membranes. In addition, many interesting properties of MOFs are connected with structural anisotropy, reversible structural changes, and

[*] D. Zacher, Dr. R. Schmid, Prof. Dr. R. A. Fischer
Inorganic Chemistry II—Organometallics and Materials Chemistry
Ruhr-University Bochum, 44870 Bochum (Germany)
Fax: (+49) 234-32-14174
E-mail: roland.fischer@rub.de
Prof. Dr. C. Wöll
Institute of Functional Interfaces (IFG)
Karlsruhe Institute of Technology (KIT)
76021 Karlsruhe (Germany)

flexibility upon interaction with guests. Consequently, the tailored synthesis of size- and shape-selected single crystals of MOFs ranging from the nano to the macro size regime is a great challenge. The same is true for the chemical functionalization and/or structural hybridization/conjugation of MOFs post synthetically, including the manipulation and positioning of these crystals as seeds or immediately as functional units on substrates. This situation bears some similarity to that of zeolite thin films[9] and zeolite nanocrystals.[10]

Looking at the nano and thin-film chemistry of porous coordination polymers more generally, that is, also including noncrystalline materials and cyanide-bridged Prussian Blue-type materials and related compounds, we provide a selection of more recent Review articles, including that by Kitagawa and co-workers on nanocrystals of coordination polymers,[11] by Mirkin and co-workers on infinite coordination polymers (ICPs),[12] and by Mallah and co-workers on functional (magnetic) coordination nanoparticles (CNPs).[13] In a previous article, we have recorded the progress on metal–organic framework thin films, largely focusing on prominent key-types of MOFs based on oligotopic organic carboxylate linkers (e.g. IRMOFs, MILs).[14] In this Review we now want to concentrate on the emerging interdisciplinary field of the surface chemistry of MOFs which links the thin-film and nanocrystal topics, a particularly rapidly developing field of MOF applications (Figure 1). We will also cover the still largely open question on the formation and growth mechanisms of MOFs. The oriented growth of MOFs with known (and interesting) bulk properties in the form of well defined, homogeneous, and smooth (ultra-)thin films or multilayers clearly involves the interaction of the MOF's building blocks with the given substrate. Also, the growth of the particular MOF on the deposited seeds or nucleating layers again is an issue of MOF surface chemistry. Essentially, the tailored growth of MOF nanocrystals in homogeneous (colloidal) solutions is directly related to the liquid-phase epitaxial growth of MOFs, that is, MOF surface chemistry at the liquid–solid interface. The interaction of the MOF building units at the surface of the growing nanocrystal in solution and the effects of certain additives (e.g. surfactants, "coordination modulators") is a quite general aspect of the surface chemistry of MOFs. MOF on MOF growth, that is, the

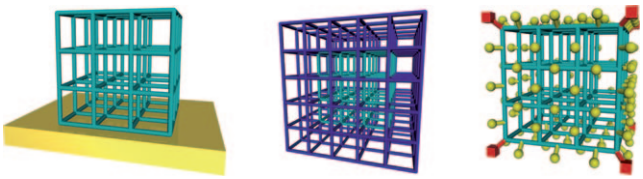

Figure 1. The range of MOF surface chemistry covered herein. left: layer-by-layer growth of thin films, middle: heterostructures, right: coordination modulation.

Denise Zacher, obtained her B.Sc. at the Universiät Duisburg-Essen and received her M.Sc. in chemistry at the Ruhr-Universität Bochum in 2006. She is currently working on her doctoral thesis under the supervision of Roland A. Fischer on the growth of metal–organic frameworks (MOF), especially thin films and nanocrystals, within the frame of the Priority Programm 1362 "Metal Organic Frameworks" of the German Research Foundation (DFG). Her work is also linked with the "SURMOF" research project of the European Union.

Christof Wöll is the director of the Institute of Functional Interfaces (IFG) of the Karlsruhe Institute of Technology (KIT). He studied physics at the University of Göttingen and received his PhD in 1987. After a postdoctoral stay (1988–1989) at the IBM research laboratories, San Jose, USA he carried out his habilitation at the University of Heidelberg. In 1997, he took over the chair for Physical Chemistry at the University of Bochum (until 2009). In 2000, he founded the collaborative research center SFB558 "Metal-Substrate Interactions in Heterogeneous Catalysis". His research interests include basic processes of surface chemistry, in particular the characterization of molecular adsorbates on metal, oxide, and organic surfaces, as well as interfacial systems chemistry.

Rochus Schmid studied chemistry at the Technische Universität München (TUM) and received his PhD in the group of Wolfgang A. Herrmann in 1997. After a postdoctoral stay with Tom Ziegler at the University of Calgary (Canada) he returned to the TUM in 1999. In 2003 he joined the group Roland A. Fischer at the Ruhr-Universität Bochum, where he finished his Habilitation in 2009 on the topic "Atomisitc Models in Materials Chemistry". Currently he is leading the research group "Computational Materials Chemistry" at the department of Inorganic Chemistry II at the Ruhr-Univerität Bochum, and is focusing on multiscale simulations using ab-initio parameterized force fields for porous coordination polymers and other hybrid materials

Roland A. Fischer studied chemistry at the Technische Universität München (TUM) and received his PhD in 1989 with Wolfgang A. Herrmann. After a postdoctoral stay with Herb D. Kaesz at the University of California, Los Angeles (UCLA), he returned to TUM in 1990, where he obtained his Habilitation in 1995. In 1996 he was appointed Associate Professor at the Ruprecht-Karls Universität in Heidelberg. In 1998 he moved to the Ruhr Universität Bochum where he took the chair in Inorganic Chemistry II. His research interests focus on Group 13/transition-metal bonds and clusters, precursor chemistry for inorganic materials, chemical vapor deposition (CVD), thin films, nanoparticles, colloids, and host–guest chemistry of porous coordination polymers (MOFs).

growth of MOFs on top of MOF single crystals (including MOF thin films) in either a homo- or a heteroepitaxial fashion completes this range of MOF surface chemistry at the solid–liquid interface. We are excluding herein all MOF-related surface chemistry involving the gas–solid interface. Rather, the intention is to present a selection of key examples as listed in Table 1 with a somewhat narrower definition of MOFs, selected from a perspective which may be useful and stimulating for the further development of the MOF field even outside of those mainstream directions which have been the topic of numerous other recent Review articles.

Table 1: Selected porous coordination polymers (PCPs) and metal–organic frameworks (MOFs) studied for their surface chemistry, multilayer and crystal-growth mechanisms.[a]

MOF formula	Surface chemistry (characterization)	Ref.
$[Ni(bipy)\{Pt(CN)_4\}]$	layer-by-layer on SAMs (IR, ellipsometry)	[23]
$[Fe(pz)\{Pt(CN)_4\}]$	layer-by-layer on SAMs (AFM, Raman)	[24]
$[Fe(azpy)\{M(CN)_4\}]$ (M=Ni, Pd, Pt)	layer-by-layer on SAMs (Raman)	[25]
$[OsL_3(PdCl_2)(PF_6)_2]$[b]	layer-by-layer on SAMs (XRR, ellipsometry)	[26]
$[Cu_3(btc)_2]$ (HKUST-1)	solvothermal on SAMs (XRD)	[18]
	layer-by-layer on SAMs (SPR, XRD)	[20]
	surface structure (AFM)	[48, 49]
	crystal growth on SAMs (AFM)	[50]
	crystal growth in colloids (TLS, XRD)	[70]
	solvothermal growth (EDXRD)	[43]
$[Zn(bdc)(bipy)_{0.5}]$ (MOF-508)	layer-by-layer on SAMs (SPR, XRD)	[31]
$[M(L)(P)_{0.5}]$ (M=Cu, Zn; L=bdc, F_4bdc, ndc; P=dabco, dpndi, bipy)	layer-by-layer on SAMs (QCM, XRD)	[38]
	solvothermal anisotropic, core–shell and BAB heterocrystals (IR, XRD)	[56, 57]
	anisotropic, surface-coordination-modulated growth (XRD, TEM, BET)	[77]
$[Fe_3O(X)_3(muc)_3]$ (X=Cl, F, OH, CH_3OH; MIL-89)	crystal growth, surface-coordination-modulated growth, thin films (EXAFS, XRD, TLS, TEM)	[44, 77]
$[Mg_2(Hcam)_3](NO_3)$	crystal growth (ESI-MS)	[46]
$[Zn_4O(L)_3]$ (L=bdc, abdc; IRMOF-1, IRMOF-3)	isotropic, AB and BAB, ABA core–shell heterocrystals (XRD, BET)	[57, 58]
	crystal growth in colloids and ligand-arrested growth (TLS, AFM, XRD)	[72]
$[Zn(mim)_2]$ (ZIF-8)	crystal growth in colloids and ligand-arrested growth (TLS, XRD, TEM, BET)	[68]

[a] Abbreviations: abdc = 2-amino-1,4-benzenedicarboxylate; azpy = azopyridine; bdc = 1,4-benzenedicarboxylate; bipy = 4,4′-bipyridine; dabco = 1,4-diazabicyclo[2.2.2]octane; dpndi = *N*,*N*′-di(4-pyridyl)-1,4,5,8-naphthalenetetracarboxydiimide; F_4bdc = 2,3,5,6-tetrafluorobenzene-1,4-dicarboxylate; min = 2-methylimidazolate; ndc = 1,4-naphtalenedicarboxylate; pz = pyrazine; muc = *trans*,*trans*-muconate; Hcam = (+)-camphoricacid. [b] L = 4′-methyl-4-{2-pyridin-4-yl-vinyl}[2,2′]bipyridyl).

2. Liquid-Phase Layer-by-Layer Growth of MOFs on Self-Assembled Monolayers

Self-assembled monolayers (SAMs),[15] are widely used as nucleation-directing templates and adhesive surfaces for numerous applications in bottom-up (chemical) nanotechnology. For example, a broad range of inorganic compounds, including calcium carbonate, lead sulfide, zinc, titanium, and iron oxides, and zeolites have been grown as thin films by employing suitably chosen SAMs as an (organic)substrate.[16] The transfer of the underlying concepts of SAM-modified crystallization to the surface-selective anchoring of MOFs and the control of the orientation of MOF crystallites deposited directly from suitably preconditioned solvothermal mother solutions was first reported our groups for $[Zn_4O(bdc)_3]$ (IRMOF-1 = MOF-5; bdc = 1,4-benzenedicarboxylate) and later by Bein and co-workers for $[Cu_3(btc)_2]$ (HKUST-1; btc = 1,3,5-benzenetricarboxylate).[17,18] Also, Bein and co-workers demonstrated the effect of SAMs on the phase-selective nucleation and growth of MOFs for hexagonal MIL-88B(Fe) in comparison to monoclinic MIL-53(Fe).[19] In addition to adapting the conventional method of $[Cu_3(btc)_2]$ deposition on surfaces, including SAMs, where the copper component and the H_3btc linker are mixed and treated under solvothermal conditions, a radically different layer-by-layer (LbL) growth mode of $[Cu_3(btc)_2]$ was demonstrated by Wöll and co-workers in 2007.[20a–c] This deposition scheme is based on the combination of the reaction partners by a sequential immersion of the substrate into beakers containing the reactants, in a stepwise fashion (Figure 2). Between individual steps the residual components are removed by rinsing the substrate with the solvent, yielding a LbL deposition.

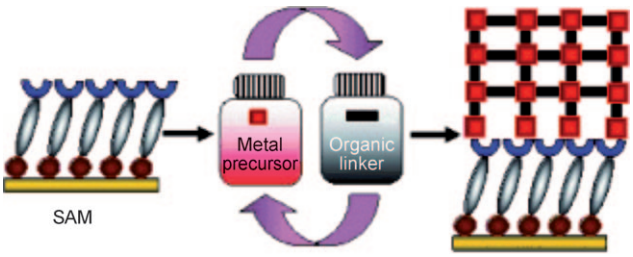

Figure 2. Layer-by-layer (LbL) growth of MOFs on SAMs by repeated growth cycles: immersion in a solution of metal precursor, washing, immersion in a solution of the organic ligand, washing. From Ref. [20c]

2.1. Growth Modes of Coordination-Polymer Multilayers

The general concept of the LbL method for bottom-up assembly of supramolecular (nano-)architectures on surfaces goes back to the fabrication of multilayer films by Irvin Langmuir and Katherine Blodgett. Later it was developed by

Decher and co-workers for the deposition of nanocomposite multilayer films of polyelectrolytes which are held together by ionic interactions and are combined with functional units, such as complexes, clusters, nanoparticles.[21] Based on these concepts, coordination polymers and/or multilayers of metal complexes connected with various linking units could be LbL deposited at SAM-modified surfaces, too. Mallouk and co-workers introduced LbL self-assembled metal–organic films in 1988, with organic modules linked by zirconium phosphonate interlayers.[22b] Early reports on the surface chemistry of structurally defined coordination polymers again date back to the work of Mallouk and co-workers in 1993 and 1994 on the growth of lamellar films of the Hofmann clathrate [Ni(bipy){Pt(CN)$_4$}] (bipy = 4,4′-bipyridine) by sequential ligand exchange reactions.[23] Inspired by this work Bousseksou and co-workers used this LbL method for the fabrication of thin films of the spin-crossover microporous coordination polymer [Fe(pz){Pt(CN)$_4$}] (pz = pyrazine) and its congeners.[24]

We will start the discussion on the LbL growth of MOFs by turning our attention to the early case of [Ni(bipy){Pt(CN)$_4$}] (Figure 3). Planar polymeric sheets are formed by square-planar tetracyanometalate ions connected by octahedrally coordinated Ni^{2+} ions. These sheets are bridged by bidentate bipy molecules attached at the apical position of the octahedral Ni^{2+} site, resulting in a 3D-structure. The LbL deposition was carried out at very low temperatures of −60 to −75 °C. Each deposition step took 6–8 h.[23c] Interestingly, the initially chosen pyridyl-terminated SAMs were separated or diluted by co-adsorption of ethylthiol (Figure 3) to roughly adjust the surface density of pyridine groups to be comparable to the density of the Ni^{2+} sites of the layers. The chemical identity of the deposited material was confirmed by comparison of the thin-film IR data with the data of a bulk reference sample. The anticipated strictly linear, self-terminated growth mode was substantiated by ellipsometry.

The measured layer spacing of the deposited material in each step was in good agreement with the spacing of the known bulk structure. However no X-ray diffraction data on the multilayer structure were reported, that is, the crystallinity and structural features of the deposited material were not fully characterized. The LbL deposition of [Fe(pz){Pt(CN)$_4$}] was carried out similarly.[24] However, direct evidence for a crystalline material was not given. These are the first pure multilayered thin-film materials that show a spin-crossover phenomenon with a hysteresis at room temperatures (Figure 4).

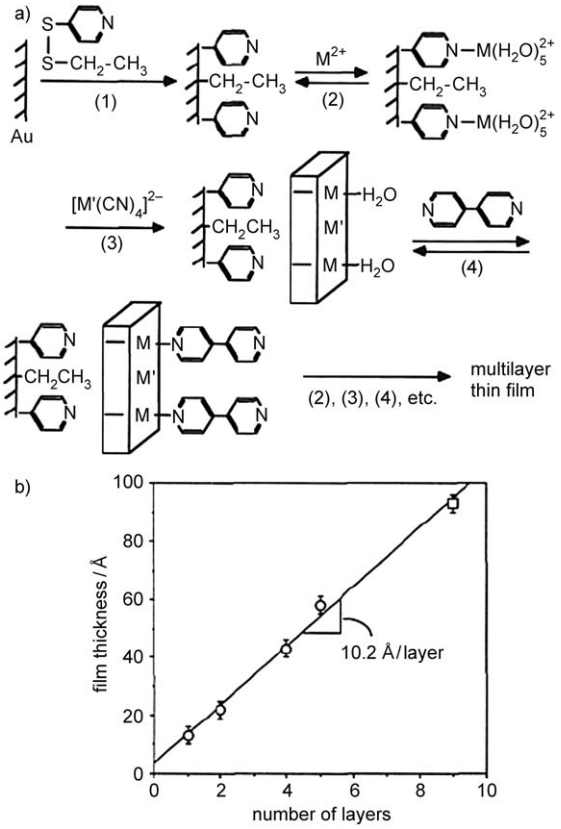

Figure 3. a) Growth scheme for deposition of multilayer Hofmann clatherate films (M = Ni, M′ = Pt). b) Ellipsometric measurements of thickness versus number of layers for [Ni(bipy){Pt(CN)$_4$}], films. Circles and square indicate two different batches of samples. The reference sample is bare gold, and the thickness of "zero" layers corresponds to the adsorbed disulfide anchoring agent. One layer refers to the sequence of adsorption step 2-3-4 in (a). Reprinted with permission from Ref. [23c]. Copyright 1994 American Chemical Society.

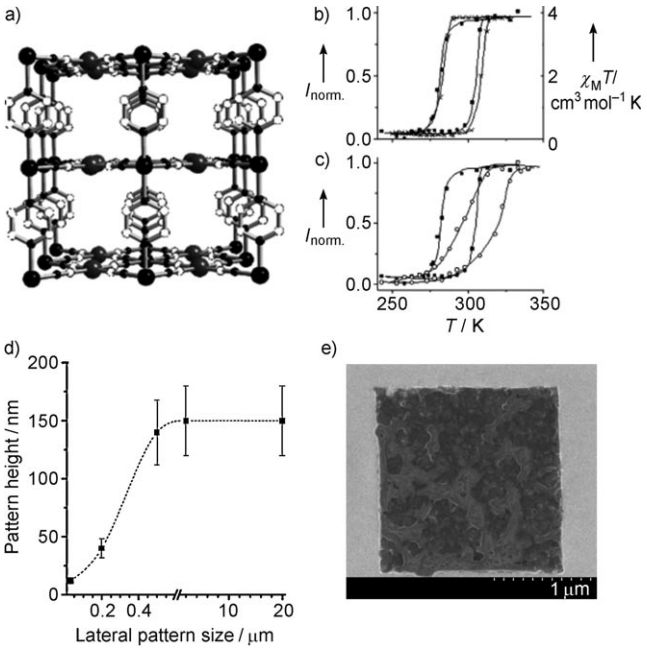

Figure 4. a) Section of the molecular structure of [Fe(pz){Pt(CN)$_4$}]. b) Temperature dependence of the $\chi_M T$ product (×; where χ_M is the molar magnetic susceptibility) and the normalized Raman intensity ratio (■; $I_{norm.} = I(1025\ cm^{-1})/I(1230\ cm^{-1})$) for [Fe(pz){Pt(CN)$_4$}] powder upon cooling and heating. c) Temperature dependence of the normalized Raman intensity ratio [$I_{norm.} = I(1025\ cm^{-1})/I(1230\ cm^{-1})$] for [Fe(pz){Pt(CN)$_4$}] powder (■) and film samples (○) upon cooling and heating. d) Pattern heights of [Fe(pz){Pt(CN)$_4$}] as a function of the lateral pattern size, after 15 deposition cycles. (The dashed line is to guide the eye.) e) Low-energy SEM image of a 2 μm pattern (ca. 150 nm thick) of [Fe(pz){Pt(CN)$_4$}]. Reprinted with permission from Ref. [24a] and [24b].

The sequential exposure of the templated mercaptopyridine SAM surface to solutions of $Fe(BF_4)_2 \cdot 6H_2O$, $[(TBA)_2M(CN)_4]$ (M = Ni, Pd, or Pt; TBA = tetrabutylammonium), and pyrazine (pz) in ethanol was also carried out at −60 °C.[24a] The low temperature was important to reduce the desorption rate of the coordinated species. The as-deposited material was characterized with Raman microscopy and magnetic susceptibility measurements (Figure 4).

A subsequent study of the deposition of $[Fe(pz)\{Pt(CN)_4\}]$ on nano- and microscale patterned SAM substrates revealed a surprising mechanistic effect of the LbL growth (Figure 4d).[24b] As the lateral size of the patterns decreased, the height of the MOF thin film decreased as well, at a constant number of deposition cycles. For 15 deposition cycles the mean height of MOF material deposited on 2 μm, 200 nm, and 50 nm large squares (fabricated by soft lithography and micro-contact printing[15]) was approximately. 150 nm, 40 nm, and 12 nm, respectively. For lateral sizes above 0.5 μm, the pattern heights remain fairly constant. This observation is quite in contrast to the early case of $[Ni(bipy)\{Pt(CN)_4\}]$ (on non-patterned SAMs) which revealed a strictly linear growth of one layer per deposition cycle (Figure 3b). This apparent discrepancy can be understood by taking into account a 3D island-growth scheme with a number of nucleation sites and limitations on the mass-transport in the case of small reaction volumes (i.e. patterned substrates with small openings in the resist). It is reasonable to expect decreased deposition rates at small nanopatterns, as pointed out for $[Fe(pz)\{Pt(CN)_4\}]$. In contrast to the idealized LbL deposition scheme of polyionic organic compounds,[21] the assembly of (weakly bound) coordination polymers is likely to involve not only adsorption steps but also desorption and re-adsorption. These processes will be accompanied by the formation of (nano-)crystallites which act as nucleation centers for preferential growth in subsequent deposition steps. Similar LbL studies on the assembly of $[Fe(azpy)M(CN)_4]$ (M = Ni, Pd, Pt) were performed by the same group using 4,4′-azopyridine (azpy) instead of pyrazine (pz).[25] A more linear growth mode was found. However, again, the number of elementary cells (layers) of $[Fe(azpy)\{Pt(CN)_4\}]$ deposited per cycle was about two-times more than expected. Considering that the Fe centers are separated by azpy by about 1.35 nm, the expected film thickness for 4 and 10 cycles is 5.4 nm and 13.5 nm, respectively. Instead, heights of 10 nm for the film after 4 deposition cycles, and around 22 nm for 10 deposition cycles were found.

At this point we draw attention to the work of van der Boom and co-workers to highlight some recent progress in the systematic investigation of bottom-up synthesis of (non-crystalline) multilayers of metal–organic coordination networks by the LbL method.[26] An instructive example is the LbL assembly of *trans*-configured $PdCl_2$ units containing layers which are interconnected by the rigid-rod chromophore 1,4-bis[2-(4-pyridyl)ethenyl]benzene.[26b] Notably, multilayer structures of this kind and related systems are not coordination frameworks comparable to MOFs, that is, they are lacking crystallinity and defined porosity. Nevertheless, the underlying principles of growing a coordination polymer at the liquid–solid interface and the use of the organic surfaces of SAMs to direct and control the growth are quite similar. Typical cases reveal the expected linear growth mode as reported for Mallouk and co-workers' films shown in Figure 3. Most interestingly, a nonlinear, self-propagating exponential growth mode was recently reported by van der Boom and co-workers for the LbL growth of multilayers of a porous 3D connected framework.[26d]

A porous hybrid structure consisting of a robust and structurally well-defined polypyridyl osmium complex, formed by the combination of $[L_3Os][PF_6]_2$ (L = 4′-methyl-4-(2-pyridin-4-yl-vinyl)-[2,2′]bipyridyl), and linked by *trans*-$PdCl_2$ units, that were introduced as $[PdCl_2(PhCN)_2]$, was grown on chlorobenzyl-functionalized float glass and silicon substrates using silane-SAMs as shown in Figure 5. The intrinsic porosity of the growing structure leads to the storage of the $PdCl_2$ component which in turn gives rise to the self-propagation of the over-all film growth. X-ray photoelectron spectroscopy (XPS) studies of the Pd/Os ratio as a function of the deposition steps confirmed a diffusion-controlled mechanism, indicating that palladium species do not diffuse out of

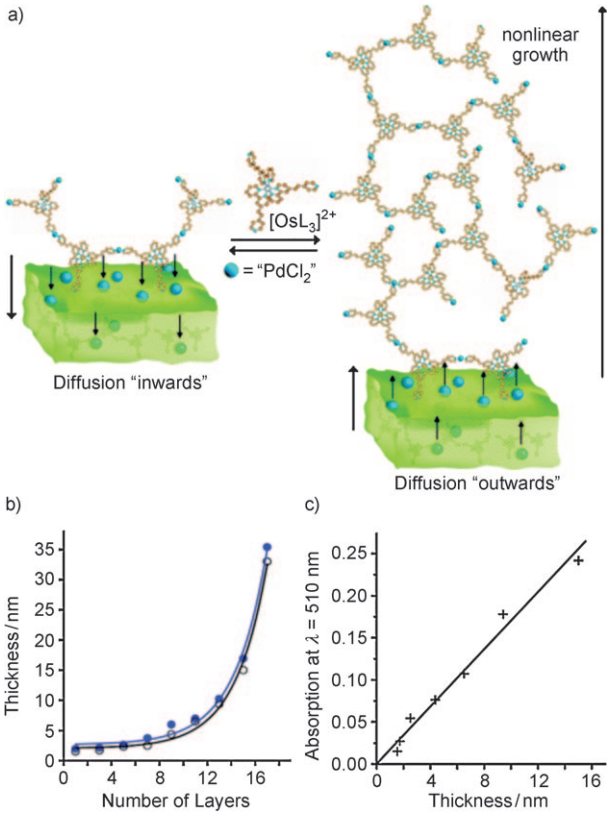

Figure 5. a) Coordination polymer multilayers formed by iterative immersion of chlorobenzyl-functionalized SAM substrates in THF solutions of $[PdCl_2(PhCN)_2]$ and $[OsL_3][PF_6]_2$. The lower layers of the continuously growing MOF are displayed as a green surface Upon immersion into the "$PdCl_2$" solution, this will be stored by diffusion in the already-grown layer. b) Exponential dependence of the multilayer thickness versus the number of layers; ellipsometry (●) and XRR (X-ray reflectivity (○)), with $R^2 > 0.986$ for the exponential fits. c) Linear dependence with the XRR-derived thickness as a function of the optical absorption at $\lambda = 510$ nm ($R^2 = 0.981$). Reprinted with permission from Ref. [26d]. Copyright 2008 American Chemical Society.

the multilayer structure into either the solution of the osmium component or into organic solvents used for the washing cycles. It was suggested that a barrier prevents loss of this essential growth component. The lack of a suitable ligand (e.g. benzonitrile) may contribute to this phenomenon. The excess of palladium stored in the molecular-based assembly is used by the system to generate another terminal hybrid layer, while retaining the structural organization. A simple numerical model, with efficiency parameters for palladium coordination and storage, was fitted to the data. Similar diffusion-related phenomena involving diffusion "into" and "out of" a deposited film leading to an exponential growth mechanism and have been observed for polyelectrolyte multilayer systems.[21b,27] These examples of LbL-grown coordination polymers or supramolecular assemblies at surfaces showing either a self-terminating and strictly linear growth, or a deviation from this scheme towards exponential growth, are limiting cases for the related LbL-growth of MOFs. Storage of the growth components, that is, SBU and linkers, are likely to occur because the growing (crystalline) films are intrinsically porous. The preference of the linear LbL growth scheme in the Hofmann clathrate type films (Figure 3 and 4) results from the microporous nature of the crystal, which is thus not prone to store growth components. Nevertheless, these examples are not typical for MOFs being deposited at surfaces in a LbL fashion.

2.2. Exceptionally Smooth Multilayer Films of the Two-Component MOF $[Cu_3(btc)_2]$

In 2007 Wöll and co-workers reported the first case of LbL-growth of a truly representative MOF, namely $[Cu_3(btc)_2]$ (HKUST-1).[20] This compound appears to be among the most commonly used MOF systems and its bulk properties have been studied in considerable detail.[28] The LbL-deposition was carried out in a similar way to the examples discussed above using a dilute ethanolic solutions of the two components copper(II) acetate ($Cu(OAc)_2$) and H_3btc in alternating cycles (Figure 2). After each step the product was washed with pure ethanol. It is important to mention that the use of zinc(II) acetate or copper(II) nitrate does not lead to the deposition of crystalline MOF material.[20c,d] In contrast to the Hofmann clathrate and the microporous spin-crossover compounds, the LbL-growth was performed at room temperature, quite similar to the deposition of the coordination multilayers of van der Boom and co-workers.[26] Two different SAM-functionalized gold surfaces, either OH- or COOH-terminated, were studied for their influence on the orientation of the deposited multilayers. No deposition was found to occur on CH_3-terminated SAMs, thus the deposition of MOFs as patterns is possible.[20b] $[Cu_3(btc)_2]$ is a good candidate to study the effect of different interactions between the SBU and the SAM template and their consequences for the growth behavior. The structure consists of a carboxylate $Cu_2(O_2CR)_4$-type paddlewheel secondary building unit (SBU) with vacant sites or substitution labile ligands at the Cu^{2+} centers. Starting the deposition with copper(II) acetate onto either a COOH- or a OH-terminated gold surface, a self-terminated linear growth was found to occur, as shown by in-situ monitoring with surface plasmon resonance (SPR) spectroscopy. Furthermore ex-situ AFM thickness measurements were carried out on [100] grown films (Figure 6).

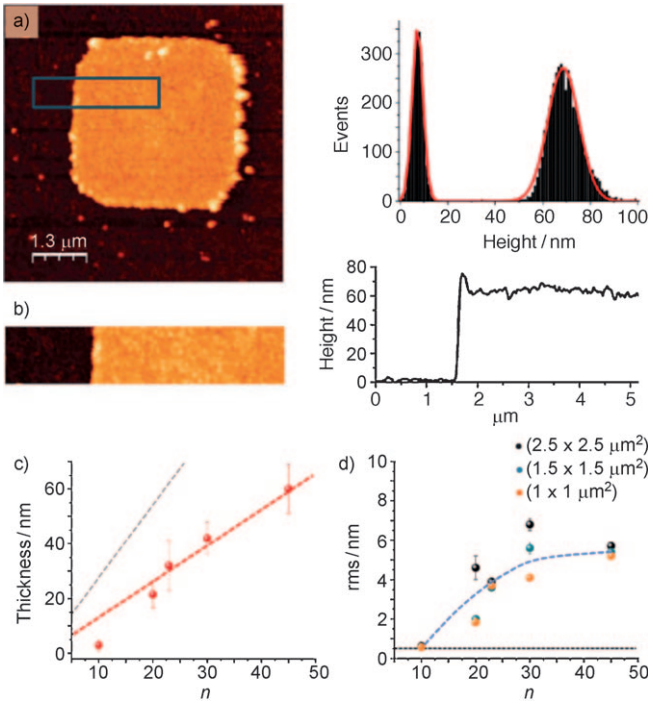

Figure 6. Top: Two different ways of measuring thickness (averaged profiles and histograms) left: a) topographic image (6.5 mm × 6.5 mm) and b) a selected area for accurate thickness estimation. right: corresponding height histogram (top) and averaged profile (bottom) calculated over the whole area in (b). Red lines in the histogram are the corresponding Gaussian fits. bottom: c) Film thickness as a function of the number of immersion cycles. The red dashed line corresponds to the proposed "half-layer" growth whereas the gray one corresponds to a one unit cell or complete layer growth (see text for details). d) Root mean square (rms) surface roughness as a function of the number of immersion cycles calculated for different scan area sizes. The black horizontal line corresponds to the rms of the starting substrate while the blue dashed line is just a visual aid. Error bars are the standard deviation values. Reprinted with permission from Ref. [20b]. Copyright 2008 Royal Society of Chemistry.

Extraordinarily smooth multilayer films of $[Cu_3(btc)_2]$ were grown in the [100] orientation on patterned COOH-/CF_3-terminated SAMs (fabricated by microcontact printing (μCP) technique). The film exhibits a surface roughness (root mean square, rms) of 5–6 nm over areas up to 100 μm^2 which corresponds to step heights of only two unit cells. SFM measurements of a series of LbL-grown multilayers demonstrate a steady thickness increase with the number of deposition cycles (Figure 6).[20b] A linear growth mode is established after 20 cycles. This observation indicates that a critical thickness is necessary to reach a homoepitaxial, self-terminated layer-by-layer growth mode. The film thickness increased by exactly half a unit cell in the [100] direction per immersion cycle. In situ AFM studies on surface-attached $[Cu_3(btc)_2]$ microcrystals deposited in the [111] direction gave

some indication that crystal growth from solvothermal solution also takes place by LbL growth (see Section 3.2).

At this point we introduce and define the acronym "SURMOF" (surface-grown metal–organic framework) to specifically address LbL grown, crystalline, oriented, and smooth multilayers and/or thin films of MOFs attached to surfaces. The XRD data recorded after 40 deposition cycles of $[Cu_3(btc)_2]$ on either COOH- or OH-terminated SAMs provided definite evidence for the formation of crystalline highly ordered thin films grown either along the [100] direction in case of COOH-termination or along the [111] direction on the OH-terminated gold surface. This behavior is in perfect agreement with similar observations reported for the direct deposition of $[Cu_3(btc)_2]$ crystallites from aged solvothermal mother solutions.[18] The orientation control induced by the SAMs was attributed to the different coordination interactions of the SAM template with the respective lattice planes of the $[Cu_3(btc)_2]$. The [100] lattice plane presents Cu_2 dimeric units which can interact with the COOH surface groups, while the [111] plane presents the apical positions of the substitution-labile Cu^{2+} centers which are likely to interact with surface OH groups (Figure 7).

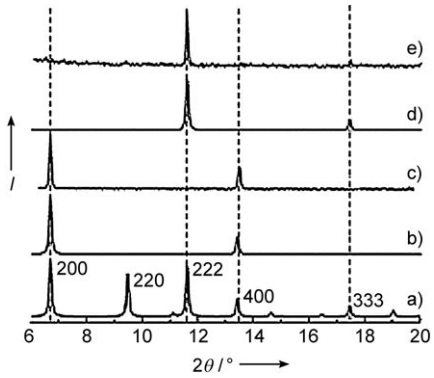

Figure 7. Out-of-plane XRD data for $[Cu_3(btc)_2(H_2O)_3]$. a) Powder, b) growth on a COOH-SAM (calculated), c) growth on COOH-SAM (experimental), d) growth on OH-SAM (calculated), e) grown on OH-SAM (experimental). Reprinted with permission from Ref. [20c].

Careful FT-IR studies on layers grown on COOH-terminated SAMs, demonstrated the absence of adsorbed growth components in the gently dried films. Adsorption of ammonia and subsequent characterization with IR and near-edge X-ray absorption fine structure spectroscopy (NEXAFS) was used to probe the gas-adsorption properties of the film. The data showed that the loading with NH_3 was similar to that observed for bulk $[Cu_3(btc)_2]$. A particular advantage of the LbL growth scheme is that it is compatible with automatic deposition instrumentation and also allows the in-situ monitoring of the growth rate. Surface plasmon resonance (SPR) spectroscopy is particularly well suited to probe the effect of various parameters on the growth efficiency, thus providing important insights into the growth mechanism.

The relevance of the metal-ion-containing component for the LbL growth of SURMOF $[Cu_3(btc)_2]$ was investigated using [100] and [111] oriented pre-grown starting multilayers of $[Cu_3(btc)_2]$ and switching between copper(II) nitrate and copper(II) acetate as the source of the Cu^{2+} ions (Figure 8).[20c]

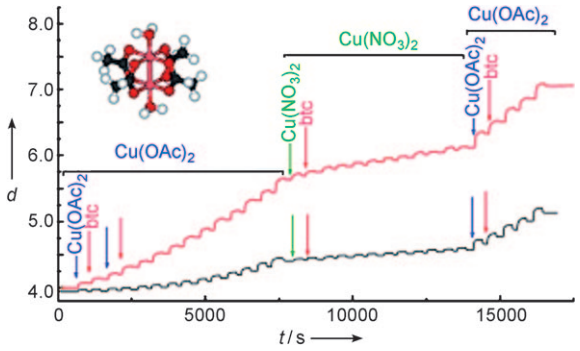

Figure 8. SPR signal as a function of time recorded in situ during the step-wise treatment of a COOH-SAM (red) and a OH-SAM (black) with $Cu(OAc)_2$, H_3btc, and $Cu(NO_3)_2$. Reprinted with permission from Ref. [20c].

Interestingly, the growth rate was very much reduced when copper(II) nitrate was used as a Cu^{2+} ion source irrespective of the orientation of the MOF thin film. Interestingly, when switching back to copper(II) acetate the growth-rate returned to the expected deposition of half a unit cell per cycle. This observation is directly related to the "SBU-controlled approach" which is particularly important for the solvothermal synthesis of MILs.[29]

The paddlewheel structure of hydrated copper(II) acetate, $[Cu_2(CH_3COO)_4(H_2O)_2]$ represents the structural motif of the btc-bridged Cu^{2+} dimers in the framework of $[Cu_3(btc)_2]$ and it is quite tempting to suggest that a simple acetate ligand-exchange reaction binds the Cu^{2+} source to the btc-terminated surface. In contrast, the diluted ethanol solution of hydrated $Cu(NO_3)_2 \cdot 3H_2O$ used for the SPR deposition experiments, does not contain similar dinuclear species and the binding constant of the mononuclear Cu^{2+} species to the surface is clearly low, as the LbL growth failed. These findings are in contrast to the observations by Attfield and co-workers (see Section 3.2).

2.3. Suppression of the Interpenetration and Oriented Growth of Multicomponent, Layer–Pillar-Structured MOFs and in the Corresponding SURMOF Heterostructures

The family of layer–pillar-structured MOFs of the general formula $[M(L)(P)_{0.5}]$ ($M = Zn^{2+}$, Cd^{2+}, Cu^{2+}, etc; L = ditopic carboxylate or other dianionic linker; P neutral pillar ligand, such as 1,4-diazabicyclo(2.2.2)octane (dabco), pyrazine (pz), bipyridine (bipy))[30] appears to be especially suited for the LbL growth of the corresponding SURMOFs as already indicated by the cyanide-linked systems described in Section 2.1. The first case study (2009) was on the LbL-growth of $[Zn(bdc)(bipy)_{0.5}]$.[31] This compound, known as MOF-508a/b, consists of a two-dimensional open framework of intercon-

nected $Zn_2(bdc)_4$ paddlewheel units, these 2D zinc carboxylate sheets are linked together by bipy pillars attached to the vacant coordination sites at the Zn^{2+}centers. The resulting huge pore size leads to the formation of an interpenetrated sublattice.[32] Not surprisingly, interpenetration is a general phenomenon in MOF chemistry and is favored for simple cubic (or tetragonal) networks as well as for sterically non-demanding SBUs and linkers.[33] A well-known example is the isoreticular series of MOFs called IRMOF-*n*, which are based on IRMOF-1 consisting of the carboxylate-bridged $[Zn_4O]^{6+}$ unit ligated with 1,4-benzenedicarboxylate (bdc). Using 4,4-biphenyl dicarboxylate (bpdc) instead of bdc leads to the formation of interpenetrated $[Zn_4O(bpdc)_3]$ (IRMOF-9).[34] Also, the phase-pure synthesis of the parent compound IRMOF-1 is complicated by interpenetration,[35] and even the recently reported IRMOF-0, $[Zn_4O(adc)_3]$, (adc = acetylenedicarboxylate) exists only as an interpenetrated structure.[36] Metal–organic frameworks were developed to provide the largest amount of coordination space possible using the least amount of material and interpenetration greatly reduces this feature. From a topological point of view, interpenetration is hard to avoid because the different networks bear translational symmetry and are therefore equivalent in the solid state. However, when a two-step LbL-growth scheme was employed using two ethanolic solutions of the starting components, one containing the metal (M) component in the form of zinc(II) acetate and the other containing an equimolar mixture of the H_2bdc linker (L) and the 4,4′-bipy pillar (P) interpenetration was avoided. A pyridyl-terminated SAM (py-SAM) of 4,4-pyridyl benzenemethanethiol (PBMT) on Au substrates was chosen to direct the growth selectively in [001] orientation, the non-interpenetrated form of MOF-508a was obtained. This result was primarily deduced from the comparison of the measured XRD data to a simulated pattern for the hypothetical non-interpenetrated bulk version (Figure 9). The Kr BET surface of the film after 55-cycles of deposition was determined to be $(627 \pm 15)\ m^2 cm^{-3}$. This volume-specific surface of the film is lower than the Kr BET bulk data of $(930 \pm 15)\ m^2 cm^{-3}$ of the interpenetrated version MOF-508a (with a corresponding standard N_2 BET surface of $821\ m^2 cm^{-3}$). The BET surface per volume for the interpenetrated and activated MOF-508a and MOF-508b is less than double that of the non-interpenetrated and activated SURMOF version, quite as expected, because the two interpenetrating networks in MOF-508a and MOF-508b are so close together, that the inner surface available for Kr adsorption is less than double the value of a single framework. When converted into surface area per weight, the value obtained of $1.010\ m^2 g^{-1}$ for the less dense, non-interpenetrated SURMOF is substantially more than the value of $660\ m^2 g^{-1}$ for the interpenetrated bulk MOF-508a and MOF-508b.[37,30f]

The orientation control of the LbL-growth of a series of layer–pillar MOFs turned out to be challenging. [Cu(ndc)-(dabco)$_{0.5}$] (ndc = 1,4-naphtaline dicarboxylate; dabco = 1,4-diazabicyclo(2.2.2)octane) was used for this study.[38] It consists of a 2D framework of $[Cu_2(ndc)_4]$ paddlewheel units, which are interconnected by dabco pillars bound to the axial positions of the Cu^{2+} centers, thus the structure is quite

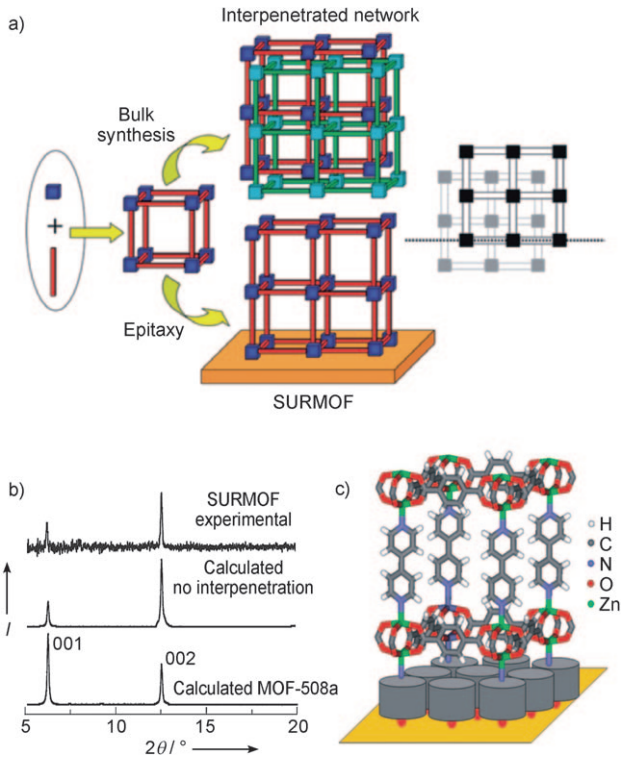

Figure 9. a) Representation of MOF synthesis concepts. By conventional solvothermal synthesis, often two equivalent networks (red and green) are formed at the same time. Using a LbL-growth scheme, the equivalence of these two networks is lifted by the presence of the substrate (dotted line in the diagram on the right) and the formation of interpenetrated networks is suppressed. b) Out-of-plane XRD patterns. Calculated diffraction pattern for an oriented MOF layer of interpenetrated type MOF-508a on the surface, the calculated diffraction pattern for an oriented MOF layer of type MOF-508a (no interpenetration) on the surface, and a 40 cycle sample grown on a pyridine-terminated SAM. c) Proposed model structure of the corresponding SURMOF, a solvent-free, non-interpenetrated pseudomorph of MOF-508a [Zn(bdc)(bipy)$_{0.5}$], grown along the [001] direction.[31]

analogous to MOF-508. The two principal growth directions [100] and [001] are perpendicular to the most-dense lattice planes (Figure 10). It would be expected that a pyridyl-terminated SAM (py-SAM) with a high affinity for the axial coordination site should promote the SURMOF growth in the [001] direction (compare with the Hofmann clathrate) and vice versa, a carboxylate-terminated SAM (COOH-SAM) should promote the 90° rotated [100] growth orientation (compare with $[Cu_3(btc)_2]$). However, this naïve approach is not enough to achieve full orientation control in multi-component MOFs. The LbL-growth scheme also had to be modified. The separation of all three growth components M, L, and P, as well as the stepwise dosing of these components in the right sequence depending on the type of SAM was necessary to reproducibly achieve oriented LbL-growth along the, [100] direction (COOH-SAM) or the [001] direction (py-SAM). For example, using the sequence $Cu(OAc)_2 \rightarrow H_2ndc \rightarrow$ dabco leads to a LbL-grown SURMOF [Cu(ndc)(dabco)$_{0.5}$] with [100] orientation. The number of deposited elementary cells (layers) calculated from the XRD data (peak profile analysis) was 30 ± 2 after 30 deposition cycles, which nicely

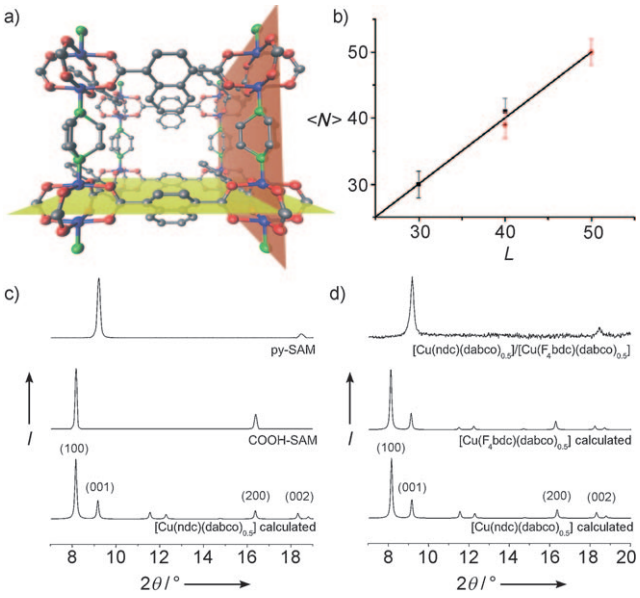

Figure 10. a) The two principle growth directions of $[Cu(ndc)(dabco)_{0.5}]$ on a surface. The [100] (red) and [001] plane (yellow) are displayed. b) Correlation of the number of unit cells N as calculated from the XRD line widths with the numbers of deposition cycles L. Solid line: expected linear dependence for the ideal self-terminated growth. Black cubes: calculated values for oriented layers deposited on MHDA-SAMs, red squares: calculated values for the deposition on py-SAM c) XRD patterns of $[Cu(ndc)(dabco)_{0.5}]$ SURMOFs (background corrected and smoothed). Bulk sample; 30 cycle three-step deposition $Cu(OAc)_2 \rightarrow H_2ndc \rightarrow$dabco on COOH-SAM (middle) and 40 cycle two-step deposition on py-SAM (top). d) Top: SURMOF heterostructure grown by LbL-deposition: XRD pattern (background corrected) of 20 cycle $[Cu(F_4bdc)(dabco)_{0.5}]$ deposited on top of a 20 cycle $[Cu(ndc)(dabco)_{0.5}]$ SURMOF in [001] orientation on a py-SAM, bottom: the calculated patterns. Each pattern is normalized to the most intensive reflection.[38]

matches a strictly linear, self-terminated growth mode. The surface roughness was determined by AFM and revealed values as low as 2.0 nm (rms) for a 20 cycle film, similar to the excellent roughness data obtained for the two-component $[Cu_3(btc)_2]$ discussed above. The extended LbL-growth scheme is currently being explored for depositing the corresponding Zn analogues, and in particular to grow SURMOF heterostructures of the from AB and ABAB , for example, with variation of the linker and pillar (L and P) or the metals M (see Section 4).[38a] Quite interestingly, the storage effects of growth components and transition from linear to exponential growth (Figure 10, see also Section 2.1) seem to be absent for these SURMOFs. Recently Kitagawa and co-workers reported the successful construction of heterostructured surface coordination polymers using the LbL technique. Though do not report a full structural model for the crystalline phase obtained.[38b]

2.4. Applications of Layer-by-Layer Grown MOFs (SURMOFs)

A first example of an integrated device using a SURMOF as the active material was developed by Allendorf and co-workers.[39] They fabricate a mechanochemical sensor from the LbL growth of $[Cu_3(btc)_2]$ on a gold-coated, SAM-functionalized microcantilever surface. The structure of $[Cu_3(btc)_2]$ is weakly responsive to the adsorption of small gaseous guest molecules, a feature that can be used as the basis of the stress-induced chemical sensing. The experiments were carried out using a film deposited in 20 cycles on a 10 μm cantilever which incorporates a built-in piezoresistive sensor for stress-based detection. The deposited materials were characterized by energy-dispersive X-ray spectroscopy and microsurface enhanced Raman spectroscopy (μSERS).[18b] No XRD data could be obtained because of the small size of the cantilever. The cantilever response was measured either for hydrated (as-synthesized) and anhydrous (activated) MOF thin films. The as-synthesized material responds rapidly and reversibly to gas-phase H_2O, MeOH, and EtOH, whereas no response to N_2, O_2, and CO_2 was observed (Figure 11). The derived H_2O resistance could be fitted to a Langmuir isotherm which agrees with the measured isotherm. In addition, Wöll and co-workers reported the possibility to use MOF thin films for measuring diffusion coefficients for small molecules, such as pyridine, within the layer.[40]

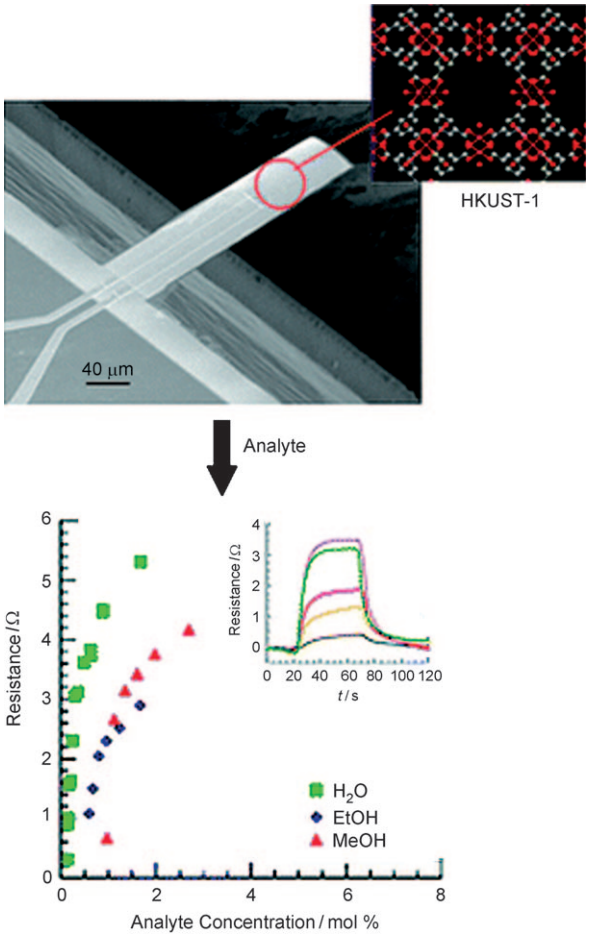

Figure 11. Response of a cantilever piezoresistive sensor to the analytes water, ethanol, and methanol diluted in N_2 (room temperature, 1 atm). Inset: Temporal response of the sensor to different H_2O concentrations: 0.18 mol%, 0.20 mol%, 0.36 mol%, 0.44 mol%, 0.98 mol%. Reprinted with permission from Ref. [39]. Copyright 2008 American Chemical Society.

To date, there are no other examples of applications of LBL-grown MOF films. Nevertheless, the thin-film spin-crossover materials discussed in Section 2.1 are very promising candidates for integration into devices.

3. Growth Mechanisms and the Role of SBUs

A general challenge in materials chemistry is understanding the mechanisms of nucleation and crystal growth on the molecular level.[41] This is very much true for MOFs, as Morris pointed out in his essay "*How does your MOF grow*?".[42] Clearly, the rational basis for advanced "design" of new MOF structures (topologies) or crystal engineered and functionalized MOFs require more knowledge about fundamental physicochemical details of the formation and crystallization of MOF materials: A better understanding of "*how complex extended network structures are assembled from simple chemical precursors in solution could ultimately permit some fine tuning of synthesis conditions to test and realize the ideas of design in synthesis*", as Millange, Walton, and co-workers point out.[43] Nevertheless, only a few studies of that kind on typical MOFs have been reported to date. These include extended X-ray absorption fine structure (EXAFS) spectroscopy and electrospray ionization mass spectroscopic (ESI-MS) studies of reactive solutions to confirm the presence of SBUs (Section 3.1), a time-resolved in-situ X-ray diffraction study and atomic force microscopy (AFM) during the solvothermal crystallization process (Section 3.2), and an in-situ time-resolved light scattering (TLS) study of colloidal solutions to monitor the formation of colloidal nanocrystals (see Section 5.1). The most direct evidence for important growth species possibly comes from in-situ AFM studies of MOF crystal growth (see Section 3.2). Again, $[Cu_3(btc)_2]$ was the system of choice and crystal growth was monitored using aged solvothermal solutions of copper(II) nitrate and H_3btc. Interestingly, these studies do not support the anticipated importance of preformed SBUs in solution for the observed 2D layer-by-layer growth.

3.1. Ex-Situ and In-Situ Spectroscopic Studies Probing the Persistence of SBUs during Solvothermal Growth of MOF Crystals

A particular important and still largely open question in MOF synthesis and crystal growth is the role of the so-called SBUs. Very few experimental studies have been performed to date. The first was reported by Walton and co-workers, who studied the formation of MIL-89(Fe), $[Fe_3O(CH_3OH)_3\{O_2C(CH)_4CO_2\}_3\cdot(CH_3OH)_6]Cl$? using a combination of ex-situ EXAFS and XRD measurements of samples taken at different reaction times.[44] Essentially they found evidence that the critical carboxylic acid bridged Fe_3O-type SBU is always present during the crystallization of this MOF. Although this was not an in-situ study, the measurements were made under close to real solvothermal crystallization conditions. In this particular case, the crystallization occurs via the initial formation of an amorphous phase which then dissolves and is completely consumed in the course of the formation of the final crystalline product. This process is analogous to that found for the hydrothermal crystallization of aluminosilicate zeolites, where an amorphous intermediate phase is commonly found prior to the formation of the zeolite.[45] ESI-MS has also been recently used by Henderson and co-workers as the tool of choice to investigate the species present during solvothermal synthesis of MOFs. Reaction of $Mg(NO_3)_2\cdot 6H_2O$ with (+)-camphoric acid (H_2cam) in acetonitrile results in the immediate formation of soluble, dinuclear $[Mg_2(Hcam)_3]^+$ ions, which could clearly be detected by ESI-MS. These dimers are three-fold paddle-wheels, which associate together through the neutral acid units to build the metal–organic framework $[Mg_2(Hcam)_3\cdot 3H_2O]NO_3\cdot MeCN$.[46] However, it should be kept in mind, that the existence of SBUs or SBU-like precursors in the mother solution may not be taken as a direct and unambiguous evidence for the role of these units as surface species at the solid–liquid interface of the growing crystal facet (see the next Section).

3.2. AFM Monitoring the Growth of $[Cu_3(btc)_2]$ from Solvothermal Solution

Atomic force microscopy (AFM) is a powerful tool to investigate crystal growth and has been applied to a range of crystalline materials including nanoporous inorganic and also inorganic–organic hybrid materials.[47] Recently $[Cu_3(btc)_2]$ was the first MOF to be studied in this way. A detailed ex-situ AFM characterization of the [111] face of single crystals of $[Cu_3(btc)_2]$ attached to a COOH-terminated SAM was reported by Szymonski and co-workers (Figure 12).[48] Freshly prepared single crystals show micrometer long terraces covered by much smaller depressions and islands with a diameter of 20–200 nm. The triangular shape of these features reflects the expected three-fold symmetry. The topographic profile 1 marked in Figure 12 shows that both islands and depressions correspond to the same change in height of about 1.5 nm which is fully consistent with expected step height (1.52 nm) on the [111] face of the $[Cu_3(btc)_2]$ crystal. By optimization of the crystallization conditions a very smooth surface was obtained exhibiting micrometer long terraces which are completely free from any screw dislocations, islands, and depressions. Exposure of the crystal to air induced erosion of the surface, after which these smooth micrometer-long terraces become covered by a very dense network of islands and depressions. In contrast to freshly prepared samples, the depth of these features corresponds, at only about 0.6–0.9 nm, to a fraction of the complete layer distance in the [111] direction.

The observed fractional height most likely corresponds to the loss of a btc linker from the [111] surface and, effectively, to the local exposure of the [222] surface of the crystal.

A similar very detailed ex-situ AFM study was independently carried out by Attfield and co-workers using single crystals of $[Cu_3(btc)_2]$ grown over 26 months from aged solvothermal solution.[49] Essentially similar data on the surface structure were obtained, however with the important

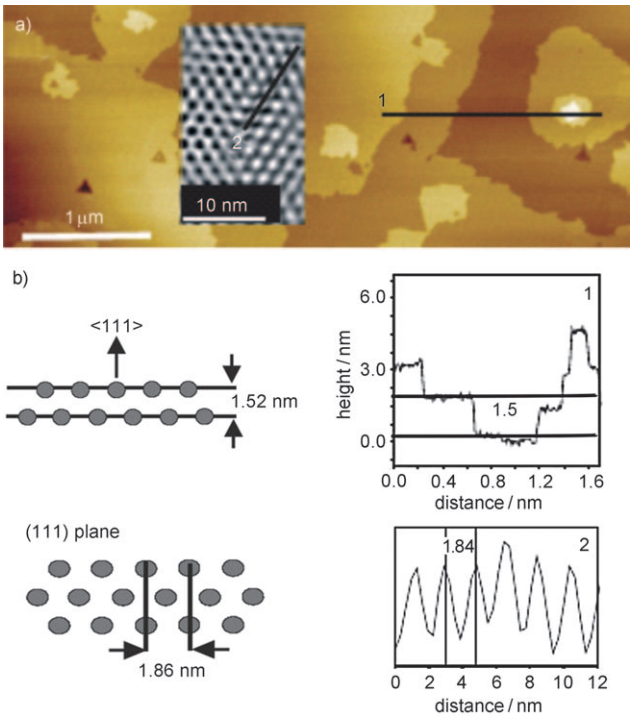

Figure 12. a) AFM images taken in air using tapping mode and in UHV in noncontact mode (inset) of the surface of $[Cu_3(btc)_2]$ microcrystals. b) Topographic profiles taken along the by black lines 1 and 2 in (a). Reprinted with permission from Ref. [48]. Copyright 2008 American Chemical Society.

difference of a high-density of screw dislocations and frequent fracturing, which result in a high density of very short terraces (ca. 100 nm). As evidenced by the frequently observed steps with a height corresponding to the multiple of 1.52/2 nm, this crystal surface also exhibits [222] termination, which makes it chemically quite inhomogenous. Attfield and co-workers were also able to perform in-situ AFM measurements.[50] They were even able to observe a single-layer growth at the [111] face by in-situ AFM measurements.[50a] This work is the first direct observation of the liquid-phase homoepitaxial growth of a MOF from a mother solution under conditions similar to those of a solvothermal process. The high-resolution AFM images of the growing [111] facet of a $[Cu_3(btc)_2]$ nanocrystal attached to a SAM surface are shown as a function of time in Figure 13c–e. The growth of the surface proceeds by a two-dimensional (2D) crystal growth mechanism. Each new layer nucleates at the same point on the crystal surface. A low supersaturation of the growth solution, a small crystal-face area, and the low-defect concentration on the crystal surface prevented additional 2D surface nucleation thus allowing the growth mode to be monitored and analyzed. The evolution of anisotropic steps that are triangular in nature and exhibit the ternary symmetry of the [111] face is nicely seen in the AFM images. Based on time-dependent AFM data, the growth model was also proposed. Note the anisotropic nature of the growth steps as a consequence of the steric requirements of layer B composed of dimeric copper-centered units and btc groups relative to the requirements of the underlying layer A (Figure 13b). This situation means

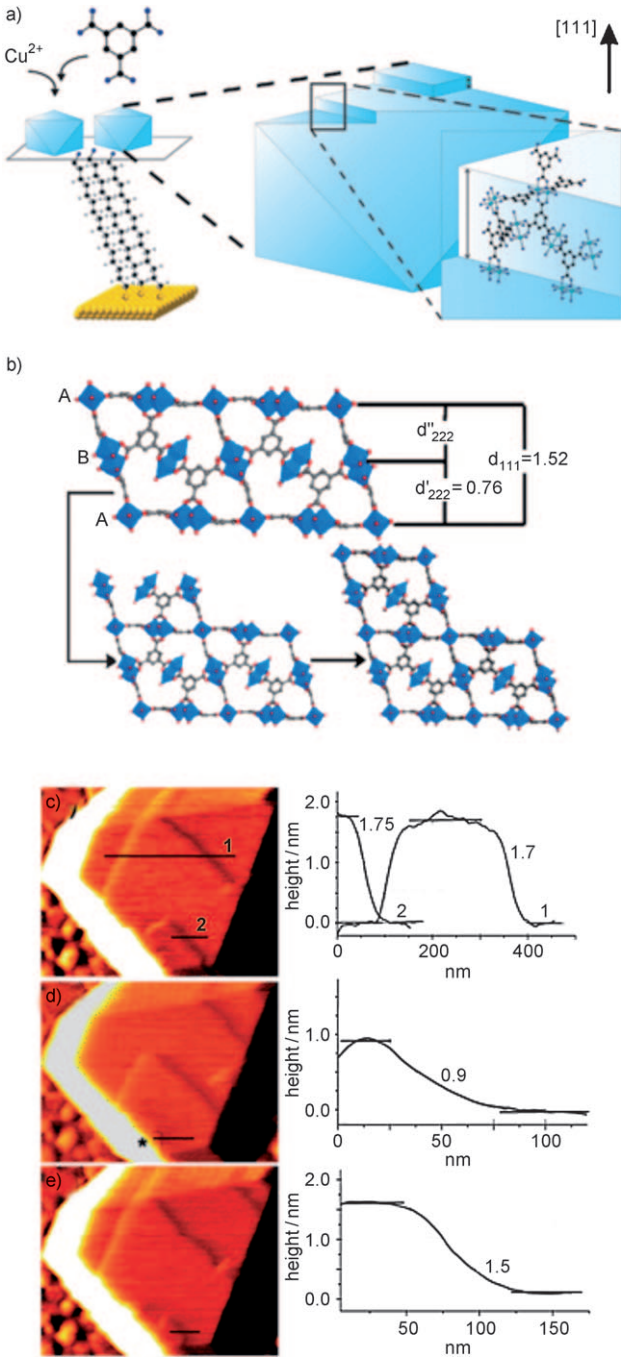

Figure 13. a) Attachment of Cu^{2+} and btc species during terrace growth on a [111] face (d_{111} steps are shown) of octahedral $[Cu_3(btc)_2]$ crystals. The crystals are attached to a 16-mercapto-1-hexadecanol-SAM (OH-termination) on a gold substrate, and grow in the [111] direction. b) The formation of a d_{111} step from the constituent d'_{222} and d''_{222} steps (The lateral size of the steps does not directly reflect those observed in (d) and (e)). c) Cross-sectional analysis of growing steps on the [111] facet and d) cross-sectional analysis of the single growth step at 77 min, and e) 79 min. Step heights were measured from height images, although deflection images are shown for clarity. Reprinted with permission from Ref. [50a]. Copyright 2009 Royal Society of Chemistry.

that the [11−2] and [2−1−1] steps are not identical and results in the steps growing at different rates in the [11−2] and [2−1−1] directions. The model suggests that a layer grows by

initial attachment of btc and Cu^{2+} species onto a stable crystal surface terminated with an A layer to form a small volume of a d'_{222} step with a metastable B layer. The attachment of additional reagent to the crystal occurs at an equal or faster rate at the newly created metastable B-layer termination of the d'_{222} step compared to the surface A-layer termination of the underlying crystal, resulting in the growth of a d''_{222} step and overall a new d_{111} step with a stable A-layer terminated surface. Essentially, Attfield and co-workers describe a layer-by-layer growth mode of $[Cu_3(btc)_2]$ from solvothermal solution under the conditions of very low supersaturation (and at room temperature). Notably, this growth scheme is somewhat in contrast to a previous in-situ study by the same authors where a 2D crystal-growth mechanism and isotropic advancement of the growth steps was observed at multiple sites across the crystal surface.[50b] This difference is explained by the use of a much larger (ca. 50 mm) crystal with a high surface-defect concentration, and hence multiple surface nucleation sites, and the use of different solvents affecting the supersaturation as well as the energetics of the crystal-growth process. However, both studies suggest that paddle-wheel SBUs of the kind $[Cu_2(btc)_4]$ are not likely to be the important species for binding to the growth site by adsorption (from this particular mother solution prepared from $Cu(NO_3)_2{\cdot}2.5\,H_2O$ and H_3btc in water/ethanol (1:1) at 75 °C, aging for 8 days and filtered). This SBU would lead to only one step/terrace height of 1.1 to 1.3 nm (or multiples), which is not observed. The relationship between these results and the data obtained by in-situ monitoring of the layer-by-layer $[Cu_3(btc)_2]$ SURMOF growth using the SBU-like paddle-wheel source $Cu_2(CH_3COO)_4{\cdot}H_2O$ instead of copper(II) nitrate (see Section 2.3) remains to be investigated.

4. Fabrication of Single-Crystal MOF Core–Shell Heterostructures

The homo- and heteroepitaxial growth of single crystals on the surface of template single-crystal substrates is a key method in (inorganic) solid-state materials science. These growth methods are of particular importance in the electronics industry,[51] where the epitaxial deposition at the gas–solid interface using chemical vapor deposition (CVD) for example is widely used.[52] Conceptually related to this area of crystal engineering, at least from the view-point of crystallography and crystal chemistry, is the liquid-phase epitaxial growth of composite or hybrid crystals of coordination polymers. Early studies on metal–organic coordination-polymer heterocrystals, for example, free-standing (not agglomerated) core–shell hybrid crystals were reported during 2000–2004 by Manson and co-workers,[53] Stang and co-workers,[54] and Hosseini and co-workers.[55] Since then, the area has been continuously expanding. However, when applying the same restrictions to the type of coordination compound of interest as applied in the preceding Sections and specifically when looking at heteroepitaxial studies of the growth of (typical) MOFs on the surfaces of MOF single-crystal cores, only a very few, but quite important and stimulating studies have appeared, most recently in 2009 and 2010.

The first synthesis of core–shell MOF single crystals by heteroepitaxial growth including a detailed X-ray diffraction analysis of the structural relationship between the shell and the core was reported by Kitagawa and co-workers.[56] Not surprisingly, a key parameter of success is choosing the "right" MOF candidates, such as the $[M(L)(P)_{0.5}]$ family mentioned in Section 2.3, which allows the variation of the metal ions M, dicarboxylate linker L, and bidentate nitrogen pillar P, without changing the original tetragonal topology (Figure 14).[30,56] The Zn-MOF, $[Zn(ndc)(dabco)_{0.5}]$, can be grown as a single crystal with cubic morphology and dimensions of hundreds of micrometers by routine solvothermal methods, but the isoreticular Cu-MOF, $[Cu(ndc)(dabco)_{0.5}]$, exists only as microcrystalline powder. However, when single crystals of the Zn-MOF were used as templates or seeds for the growth of the Cu-MOF, and were immersed into the solvothermal mother solution of $CuSO_4{\cdot}5\,H_2O$, H_2ndc, and dabco in toluene/methanol (1:1), and the solution was heated to 393 K, a single-crystalline shell of the Cu-MOF was deposited on the faces of the almost cubic Zn-MOF core crystal. The interface between the two MOF crystals was characterized by high-resolution X-ray diffraction and reciprocal-space mapping. The structural model for the [001] face (Figure 14 d) shows the in-plane rotational epitaxial relationship between core and shell crystals. Because the lattice constant of the shell crystal is significantly smaller than that of the core crystal, in-plane rotational epitaxial growth can compensate for the difference in the lattice constants. Such rotational crystal growth does not occur at the [100] surface because the lattice of the shell crystal almost matches that of the core crystal along this direction. It was noted that since the carboxylate linker L and the nitrogen pillar P are exchangeable in this $[M(L)(P)_{0.5}]$ system, and because functional groups can be introduced, it should be possible, by careful choice of the components, to correlate the resulting interfacial structure and with novel functions of the hybrid MOF crystallites, for example as a sieve for the separation or selective passage of guest molecules.

The zinc system $[Zn(L)(P)_{0.5}]$ (L = ndc, P = dabco or *N*,*N*′-di(4-pyridyl)-1,4,5,8-naphthalenetetracarboxydiimide, dpndi) was used by Kitagawa and co-workers to fabricate block MOF heterocrystals by anisotropic hybridization and face-selective epitaxial growth (Figure 15).[57] The (homo-)epitaxial growth of a second MOF crystal B on a core MOF crystal A led to a BAB block crystal. By using the same layer-ligand L, ndc, for crystal hybridization, epitaxial growth on two [001] surfaces of the core crystal no longer requires the use of a pillar ligand P with the same lattice constant, thus a variety of pillar ligands is available for use, with the possibility of forming pores at the interface. The epitaxial relationship of the hybridized BAB crystals was characterized by XRD. This concept will open the way to the fabrication of multifunctional MOFs in which several porous properties are integrated into a single crystal.

These fascinating perspectives could also apply to the $[M(L)(P)_{0.5}]$-type SURMOFs discussed in Section 2.3. However, the dimensions of the hetero-SURMOFs are much smaller, on the order under 100 nm, compared to the over 10 μm for the free-standing hybrid crystals. In principle, only few alternating layers of MOF A and MOF B can be grown on

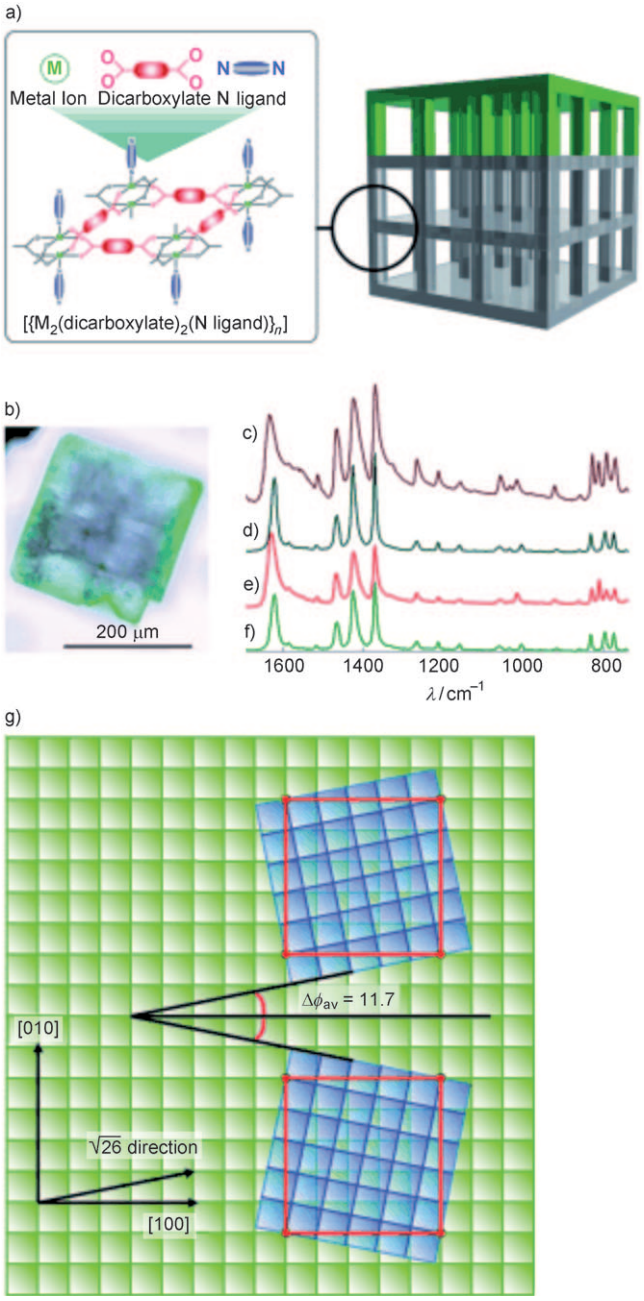

Figure 14. a) The structure of the series of frameworks $[\{M_2(L)_2(P)\}_n]$ (M = Zn, Cu) and the heteroepitaxial growth of the Cu-MOF on top of the Zn-core MOF. b) Optical microscopic image of the sliced core–shell crystal. c)–f) IR spectra by microscopic attenuated total reflection (ATR) measurement of the colorless part (c), the greenish part (d), the powder sample of the Zn-MOF (e), and the powder sample of Cu-MOF (f). g) Schematic model of the structural relationship between the core lattice and the shell lattice on the [001] surface. The red lines indicate the commensurate lattice between the core lattice (green, Zn-MOF) and the shell lattice (blue, Cu-MOF): the (5×5) structure of the core crystal or the $(\sqrt{26} \times \sqrt{26})$ structure of the shell. Two Miller domains of the shell crystal are grown on the [001] surface of the core crystal while maintaining the rotational angle ($\Delta\Phi_{av} = 11.7°$), which corresponds to the $\sqrt{26}$ direction of the [001] surface. The inset shows the chemical structure of the [001] surface. Reprinted with permission from Ref. [56].

top of each other with (possibly) abrupt interfaces in case of SURMOFs. However, the number of layers of MOF B grown epitaxially on top of MOF A can be precisely adjusted by the LbL growth. Furthermore, the orientation of the SURMOFs relative to the underlying substrate can be controlled and patterned deposition allows integration into devices.

The interaction of hetero-SURMOFs with guest molecules, that is, gas absorption as a function of the interface and the hetero-SURMOF orientation, can be monitored by in-situ

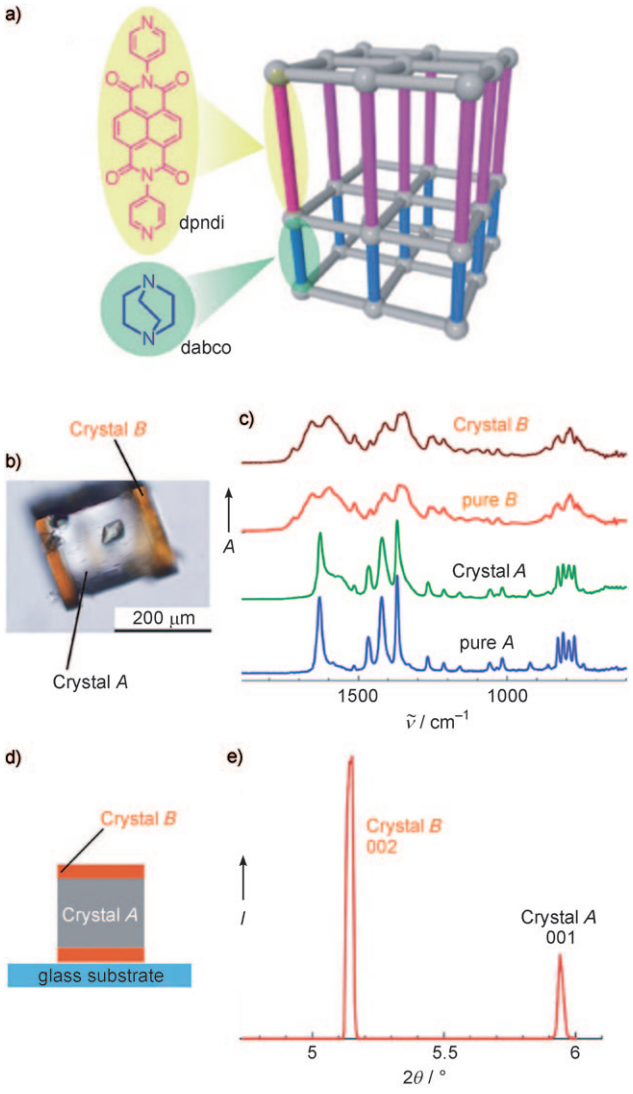

Figure 15. a) Anisotropic homoepitaxial growth of a second $[M(L)(P)_{0.5}]$ framework, $[Zn(ndc)(dpndi)_{0.5}]$ (crystal B), on the core framework $[Zn(ndc)(dabco)_{0.5}]$ (crystal A). b) The optical microscopic image of the anisotropically hybridized crystal of A and B. c) The infrared spectrum by ATR measurement of the orange part of the hybrid crystal shown in (b; crystal B), the single-crystal sample of pure B, the colorless part of the hybrid crystal shown in (b; crystal A), the single-crystal sample of pure A. d) Schematic illustration of configuration of a hybrid crystal, on a glass substrate for synchrotron X-ray diffraction measurements. e) The θ–2θ scan of the hybrid crystal at the initial position (w = 901). Two peaks assigned to the [002] Bragg peak for crystal B, ($2\theta = 5.1261$) and the [001] Bragg peak for crystal A ($2\theta = 5.9461$) were obtained simultaneously in the same scan. Reprinted with permission from Ref. [57]. Copyright 2009 Royal Chemistry of Society.

SPR (surface plasmon resonance) and QCM (quartz crystal microbalance) techniques. With similar goals in mind, Matzger and co-workers[58] and Jeong and co-workers[59] reported on MOFs@MOFs core–shell single-crystal structures (Figure 16 and 17) based on Yaghi's $[Zn_4OL_3]$ IRMOF series[60] (L = functionalized, linear rigid-rod dicarboxylates, for example, bdc for MOF-5 (= IRMOF-1) and 2-aminobenzene-1,4-dicarboxylate (abdc) for IRMOF-3) by using different linkers L instead of different metals. Mixing two different linkers such as bdc and abdc with (almost) the same structure and coordination properties lead to a random distribution of the two linkers within the isoreticular framework. The key finding of these random linker incorporation studies was the dependence of the composition and the surface area on the ratio of the two linkers. This concept has recently been systematically expanded.[61] A sequential growth similar to that of $[M(L)(P)_{0.5}]$ resulted in nesting of the individual cubic frameworks IRMOF-1 (A) and IRMOF-3 (B) to give isotropic core–shell porous structures of the type AB or BA and ABA or BAB similar to the anisotropic heterostructures described above (Figure 16). This method demonstrates the possibility to design more complicated architectures in which, to approach a central porous space, a guest must first pass through one or more additional phases. Such systems should offer the possibility to tune the kinetics of guest uptake and release, as well as provide multistage catalyst beds in a single material. The same system IRMOF-3/IRMOF-1 was selected by Jeong and co-workers[59] to fabricate the first example of a heteroepitaxially grown hybrid-MOF membrane (Figure 17). Essentially the same solvothermal synthesis concept as used by Matzger and co-workers[58] was applied using microcrystals of IRMOF-1 as seeds for the subsequent growth step of IRMOF-3 or vice versa to yield the core–shell type heterostructure. The heteroepitaxial relationship (almost matching lattice parameters) was studied by X-ray diffraction techniques.

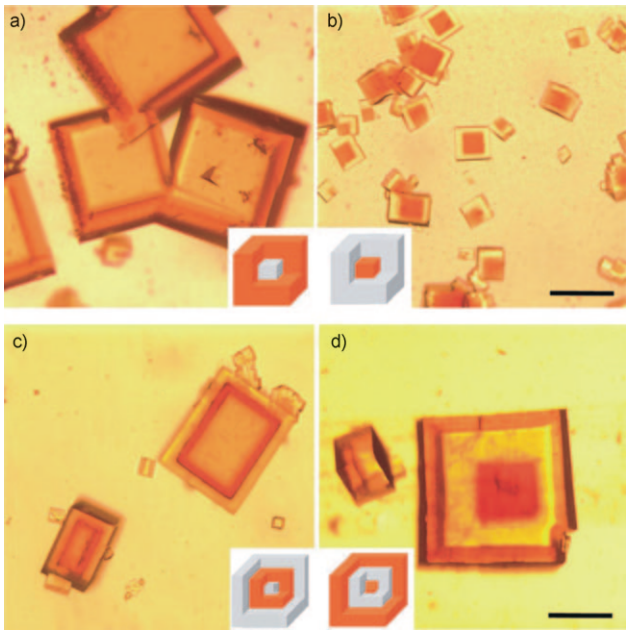

Figure 16. Microscope images and schematic views (insets) for core–shell heterostructures formed from IRMOF-1 (gray; also denoted MOF-5) and IRMOF-3 (orange):[58] a) IRMOF-3(shell)@IRMOF-1(core), b) IRMOF-1(shell)@IRMOF-3(core), c) IRMOF-1(2nd layer)@IRMOF-3(1st layer)@IRMOF-1(core), d) IRMOF-3(2nd layer)@IRMOF-1(1st layer)@IRMOF-3(core). Scale bar: 200 mm. Reprinted with permission from Ref. [58]. Copyright 2009 Royal Society of Chemistry.

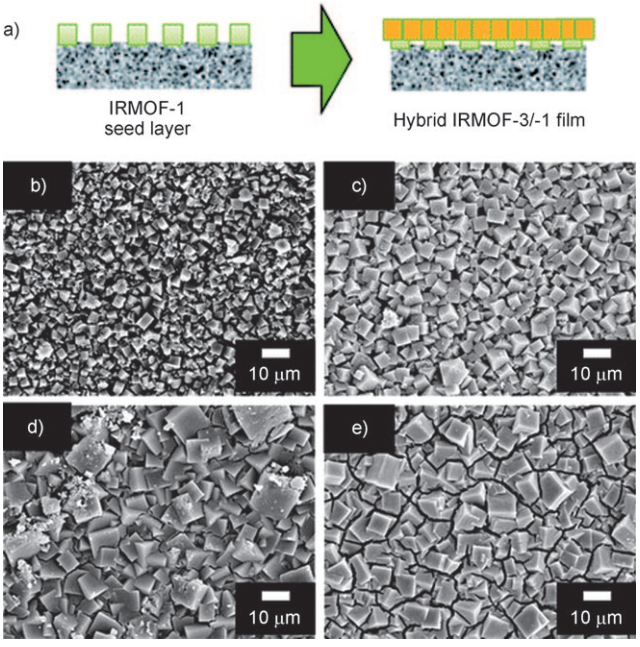

Figure 17. a) Heteroepitaxially growth of IRMOF-3 on the surface of an IRMOF-1 seed layer on a porous support. b)–e) SEM images of an IRMOF-1 seed layer (b), and IRMOF-3/IRMOF-1 hybrid films grown for 1 h (c), for 2 h (d), and for 3 h (e). Reprinted with permission from Ref. [59]. Copyright 2010 American Chemical Society.

5. Surface-Controlled Growth of Nanocrystalline MOFs in Colloidal Solution

In contrast to the massive amount of literature on synthesis, structure, and properties of microcrystalline bulk-phase MOF materials, there has been much less focus on the tailored fabrication of well-defined MOF crystallites in the sub-micron size regime or on their size-, shape-, and surface/volume-dependent properties in comparison to the bulk-phase macrocrystals. Quite recently, with the perspective of biological (pharmaceutical) applications of MOFs ("Bio-MOFs"),[62] there has been an increase in interest in this area, primarily pushed by Férey and co-workers (drug storage and long time release)[63] Morris and co-workers (gaseous signal molecule delivery, for example, NO),[64] and Lin and co-workers (bioimaging).[65] As already mentioned in the Introduction, Mirkin and co-workers coined the term ICP (infinite coordination polymer) for those nanoscale (porous) coordination polymer materials which are typically lacking long-range crystalline order and maybe more or less related or even structurally different from their parent MOF materials.[12] Typically nano-MOFs of the kinds summarized by Mirkin and co-workers are synthesized by the adaptation of colloid chemistry techniques developed for many classic

inorganic materials 1) solvent-induced size-selective precipitation, 2) synthesis in microemulsions, and 3) arrested growth during solvothermal synthesis. Nano-MOFs prepared by solvent-induced precipitation tend to be amorphous and may be regarded as ICPs in a narrower sense,[12] while synthesis in microemulsions[65] and arrested-growth techniques[63] usually lead to chemically more defined (nano-)crystalline materials. In addition microwave[66] and ultrasound techniques[67] were used for rapid synthesis of (nano-)crystalline MOFs. For example, Gref and co-workers obtained nanoscale agglomerated powder materials of MIL-53, MIL-88A, MIL-88B, MIL-89, MIL-100, and MIL-101-(NH_2) simply by control of concentrations, temperature, and growth time during the standard solvothermal synthesis under autogeneous pressure in (small) teflon autoclaves with or without the addition of biocompatible surfactants, such as monomethoxy aminopoly(ethylene glycol).[63a] The particle size distributions were generally quite broad and depend on the type of MOF. They range from 50–500 nm and even to mm scale depending on the conditions. In this context there is a report by Lin and co-workers on post-synthetic modifications of 100–200 nm sized MIL-101(Fe) (octahedral) nanocrystals (for imaging and drug delivery).[65e] The particularly interesting aspect in terms of MOF surface chemistry was the post-synthetic (after nano-MIL loading with imaging labels or drugs) coating of the MIL nanoparticles with a silcate shell to form core–shell structures of the kind MIL@SiO_2 without decomposing the MIL crystallite. The release of the adsorbed molecules from the MIL host though the (porous) SiO_2 shell was monitored by fluorescence spectroscopy and expectedly showed retarded release in comparison to the non-coated MIL nanoparticles. A similar strategy was used to silica coat nano-MOFs of the composition $[Ln(bdc)_{1.5}(H_2O)_2]$ (Ln = Eu^{3+}, Gd^{3+}, or Tb^{3+}), to form $[Gd(bdc)_{1.5}(H_2O)_2@SiO_2]$ which were synthesized using a reverse microemulsion system.[65a]

However, the kind of surface chemistry of MOFs, which is involved in the context of biological or medical applications for "BioMOFs",[62] is not particularly related to the surface-chemical perspectives of MOFs discussed in the previous Sections. We therefore do not want to attempt to cover comprehensively the emerging chemistry of MOF nanoparticles in a general sense and again refer to the current Reviews by Mirkin and co-workers[12] and Férey and co-workers.[2,62] Rather, we restrict the discussion herein to those cases of nanocrystal MOF chemistry which directly show the influence of surface-attached ligands or additives on the size and shape evolution of the growing MOF nanoparticles. This restriction relates to the mechanism and kinetics of the growth of "freestanding", that is, not agglomerated single MOF nanocrystals in colloidal solution and complements the examples of surface and interfacial chemistry of MOFs given in the previous Sections.

5.1. Monitoring the Growth of Homogeneously Nucleated MOF Nanoparticles

Few studies have been performed with in-situ monitoring of the growth of nanoscale MOF crystals. The method of choice for these studies was time-resolved static light scattering (TLS; at a range of scattering angles). Rapid room-temperature synthesis of very small and uniform (40 ± 3) nm sized nanocrystals of the prototypical ZIF-8 material, [Zn-$(mim)_2$] (mim = 2-methylimidazolate) occurred by simply pouring a methanol solution of $Zn(NO_3)_2 \cdot 6H_2O$ into a methanol solution of Hmim.[68] The molar ratio of zinc(II) nitrate, Hmin, and methanol was 1:8:700 (Figure 18). It is important to have Hmim in large excess to the zinc source, contrary to reported methods for the usual solvothermal synthesis that were designed to produce large microcrystals and used the zinc salt and Hmim in a molar ratio 1:2.[69] The initially formed particles were characterized by XRD and HRTEM revealing the expected parameters of the ZIF-8 bulk phase with some line broadening of the diffraction peaks as a result of the nanoscale coherence length of the crystallites. The nanocrystals were of rhombic dodecahedral shape. As revealed by in-situ TLS studies, particles with a radius of gyration R_g of approximately 20 nm were rapidly formed, within 130 s after mixing the component solutions. During the following growth period of 170 s, the weight-averaged particle mass M_w increased further, whereas the corresponding size of particles remained essentially constant in this growth period. This observation is explained by means of the different averages of the R_g and M_w values, respectively. A situation with the size values staying constant but with mass values increasing is observed if single particles grow very fast compared to the duration of the time-resolved experiment. Beyond 300 s, the growth process accelerated because of aggregation of the primary particles. The correlation between the radius of gyration and the corresponding mass in this regime of agglomeration led to a power-law behavior for $R_g \approx M_w^a$ with the parameter a of $0.65 < a < 0.75$ indicating a fractal dimension $1/a$ that corresponds to a loose aggregate of primary nanocrystals as observed by TEM. The thermal stability of the nano-ZIF-8 material which undergoes decomposition at 200 °C (in air) was significantly lower than the bulk material, which is stable up to 400 °C (in air). Also the BET surface and micropore volume reduced to 962 $m^2 g^{-1}$ and 0.36 $cm^3 g^{-1}$ (ZIF-8: 1630 $m^2 g^{-1}$; 0.64 $cm^3 g^{-1}$). Clearly, the nano-ZIF-8 still contains adsorbed species even after activation (i.e. the structure contains more defects than the bulk-phase). The auto-arrested growth behavior was explained by taking into account the large excess of the Hmin linker which is quite likely to bind to the surface of the primary ZIF-8 nuclei. Deprotonation of Hmin and growth are driven by the relative gain of lattice energy during the crystallization of ZIF-8. This gain of lattice energy decreases with increasing the volume/surface ratio. Thus, excess of neutral Hmim terminates growth and stabilizes positively charged nanocrystals (the Zn^{2+} charge is not fully compensated; Figure 18). This model is nicely supported by the measured ζ-potential (+55 mV) of the stable dispersions of ZIF-8 nanocrystals in methanol. A somewhat related scenario was found for

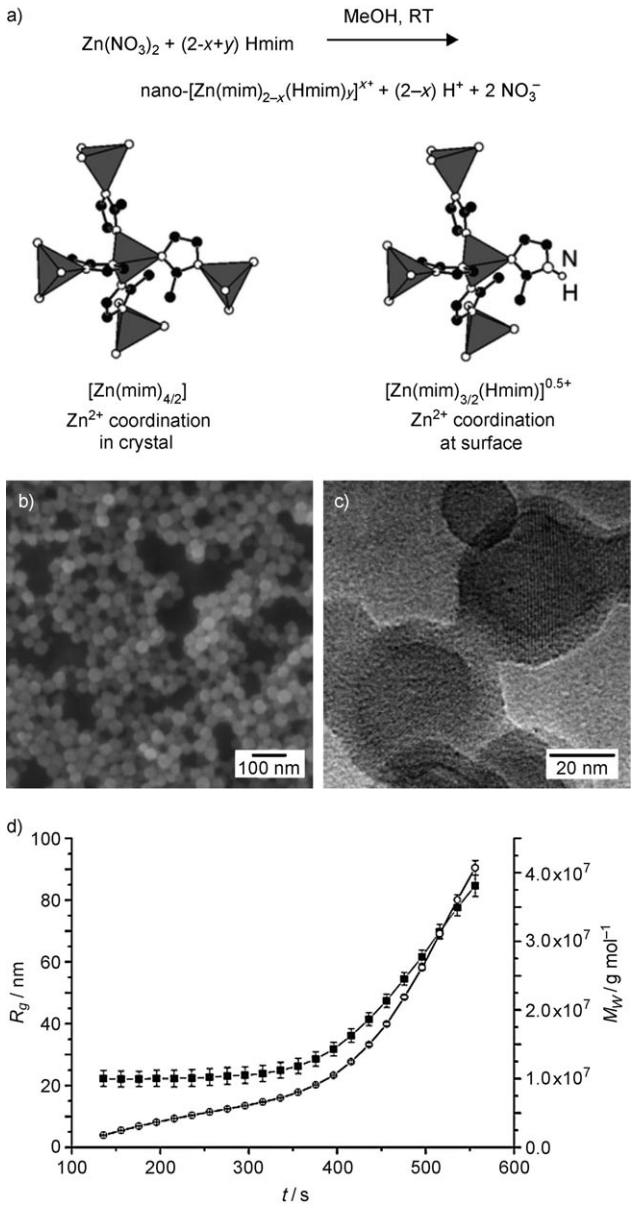

Figure 18. a) Synthesis of nano-ZIF-8 by auto-induced arrested growth using a large excess of linker Hmin. middle: b) SEM micrograph, c) HRTEM micrograph showing nanocrystals that exhibit lattice fringes of approximately 1.2 nm that correspond to the [110] family of planes. d) Monitoring of the growth and aggregation of the primary formed small ZIF-8 nanocrystals of $R_g \approx 20$ nm (Zn/Hmim/MeOH 1:5:1000). Radius of gyration R_g (■) versus time and weight-averaged particle mass M_w (○) versus time. Reprinted with permission from Ref. [68]. Copyright 2009 American Chemical Society.

homogeneous nucleation and growth of HKUST-1, $[Cu_3(btc)_2]$, again monitored by TLS.[70] A preformed, diluted solvothermal mother solution of copper(II) nitrate trihydrate and H_3btc in molar ratio 3:2 in a water/ethanol (1:1) solvent mixture was rapidly cooled from 85 °C to 25 °C and directly filtered into the scattering cells and studied by TLS. In addition, ex-situ SEM studies at different stages of growth were performed by "fishing" out samples of nanoparticles with gold surfaces coated with a sticky SAM surface (COOH-termination, See section 2.3).

The accumulated data support a mechanism for $[Cu_3(btc)_2]$ growth from solvothermal solutions involving continuous slow nucleation in parallel to fast crystallite growth. Thus, the mother solution contains small and large crystallites in a bimodal size distribution. Interestingly, under the conditions of the experiments the limiting particle size was about 200 nm beyond which aggregation takes place. This mechanism seems also to be important for the real solvothermal synthesis of $[Cu_3(btc)_2]$ as Millange, Walton, and coworkers revealed by the use of time-resolved energy-dispersive X-ray diffraction (EDXRD; Figure 19).[43] This particular technique has been used successfully for the in-situ study of the crystallization of a variety of inorganic materials and has now been used to study MOF crystallization for the first time.[43,71] Data analysis was performed using the empirical

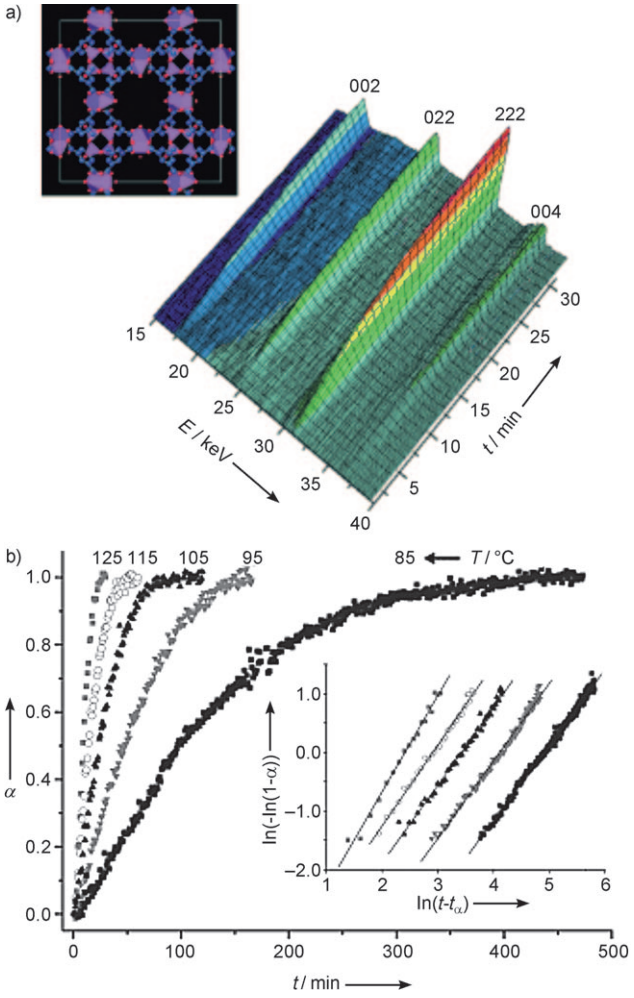

Figure 19. a) Time-resolved in-situ EDXRD data measured during the crystallization of $[Cu_3(btc)_2]$ at solvothermal conditions at 125 °C. The Bragg peaks are indexed on an F-centered cubic unit cell with $a = 26.34$ Å. Inset: view of the structure of $[Cu_3(btc)_2]$ with five-coordinate Cu as pink polyhedra, C blue, O red. b) Kinetic analysis of the crystallization of $[Cu_3(btc)_2]$: plot of extent of crystallization curves against time obtained by integration of the [222] Bragg peak in the EDXRD data. Inset: analysis by the method of Sharp and Hancock to test fitting to the Avrami–Erofe'ev nucleation-growth crystallization model $\alpha = 1 - \exp\{-(k(t-t_0))^n\}$ with lines that are the result of linear regression analysis. Reproduced with permission from Ref. [43].

Avrami–Erofe'ev model, which is widely applied for nucleation-growth process from a homogeneous medium, such as crystallization from a solution or gel, and it allows rate constants to be extracted and compared when reactions conditions are varied. The value of n, the Avrami exponent, gives some indication of the mechanism of crystallization, in particular the balance of the rates of nucleation versus crystal growth. The extracted value $n = 1.5$ suggests that crystallization is controlled largely by the formation of nucleation sites, rather than by diffusion of reactive species to the sites or of crystal growth itself. This finding fits to the data obtained from the TLS studies of colloidal $[Cu_3(btc)_2]$[70] and the results on the growth of thin films and single crystals of $[Cu_3(btc)_2]$ on SAMs as discussed in Sections 2.2 and 2.3.

However, this mechanism of rate-limiting nucleation and fast growth is certainly not a general model for MOF crystallization. Another representative MOF family may behave quite differently, as is the case with $[Zn_4O(bdc)_3]$ (IRMOF-1), which was studied by TLS, too. In this case, both M_w and R_g continuously rise until precipitation takes place at a particle size over 350 nm.[72] For IRMOF-1, homogeneous nucleation was found to be fast relative to the subsequent growth step of the crystallites and the over-all situation is dominated by the continuous growth of the initially formed IRMOF-1 nuclei. TLS does not only yield the particle size and molar mass. If the particles are larger than 100 nm, TLS also provides information about the shape of the particles. The logarithm of the scattered intensity $I(q)$ in its normalized version $P(q) = I(q)/I(q{=}0)$ displays characteristic oscillation, that is, minima for $P(q)$ in the case of high symmetry (spheres, cubes, rods) and very narrow size distribution.[73] In Figure 20, an example is shown for particles of a typical size of 320 nm. A first minimum occurs around $q = 0.01\ nm^{-1}$, and a second one around $q = 0.02\ nm^{-1}$. Clearly IRMOF-1 grows in the shape of perfect cubes from the very beginning. Nucleation and growth seem to be quite effectively separated, since the characteristic features of $P(q)$ are only observed for almost monodisperse samples. This growth mechanism allows size-selected particles to be trapped at a certain stage of their growth through the addition of a surface-capping reagent. This procedure is similar to that employed in semiconductor quantum-dot synthesis by colloidal methods.[74]

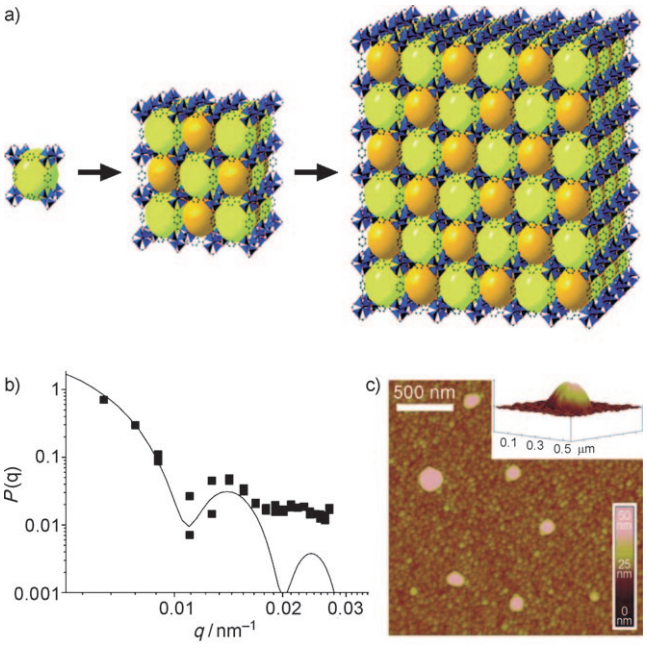

Figure 20. a) Schematic representation of IRMOF-1 nanocrystal growth. b) Particle scattering factor of IRMOF-1 nanocrystals. The radius of gyration of the crystals is 320 nm. c) Arrested growth of IRMOF-1 crystallites by addition of perfluoromethylbenzenecarboxylate (pfmbc) at a molar ratio of bdc/pfmbc of 1:5 and AFM imaging after depositing the particles by "fishing" in the diluted colloid using a COOH-terminated substrate. Reprinted with permission from Ref. [72]. Copyright 2007 American Chemical Society.

As a capping agent perfluoromethylbenzenecarboxylate (pfmbc) was chosen, which is likely to bind to vacant edges of surface-exposed Zn_4O sites (Figure 20). The respective molecular reference compound $[Zn_4O(pfmbc)_6]$ is known.[75] The capping agent pfmbc was shown to compete with bdc for coordination to the $[Zn_4O]^{6+}$ surface units and acted also as an etching agent as indicated by the reduction of the initial particle size $R_g = 300$ nm down to $R_g = 150$ nm. These resulting pfmbc-capped particles yield quite stable colloids over several weeks at 25 °C in contrast to the uncapped case, where sedimentation occurs by this time.

It is important to note, that the formation mechanisms and crystallization processes of MOFs as soft inorganic–organic hybrid materials, which have similarities with both inorganic solid-state structures and networks, as well as with organic polymers which tolerate disorder, are certainly complex and possibly as diverse as the class of compounds itself. This includes of course the surface chemistry of the individual growth intermediates at the liquid–solid interface of a MOF.

The second system studied by EDXRD was the iron(III) terephthalate with the MIL-53 structure, $[Fe^{III}(OH,F)(bdc)\cdot H_2O]$.[43] It turned out that MIL-53 crystallization is proceeded by the transient appearance of another crystalline phase related to MOF-235,[35] in which trimers of iron(III) oxy-octahedra are linked by terephthalate ligands, and trapped within the porous network. This result shows how sensitive the system is to conditions and the choice of the components including solvent, counterions, and additives.

5.2. Coordination-Modulated, Shape-Selective Synthesis of MOF Nanoparticles

The use of capping agents, introduced by Fischer and co-workers[72] (Figure 20), for blocking MOF nanocrystal growth was recently extended by Kitagawa and co-workers to a more general concept of surface coordination modulation which allows control of the nucleation and shape evolution of $[M(L)(P)_{0.5}]$-type MOFs (Figure 21).[76] The solvothermal growth of $[Cu(ndc)(dabco)_{0.5}]$ was modulated by adding various amounts of acetic acid which competes at the different stages of nucleation and growth with the H_2ndc for coordination at the Cu^{2+} sites of the growing MOF. The obtained nanorods grew in the [001] direction of the framework by the fusing of small nuclei by coordination through the

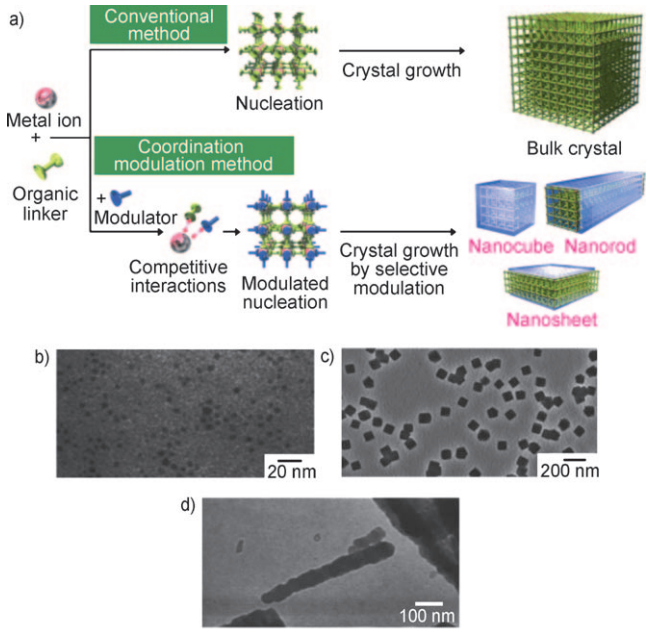

Figure 21. a) Coordination-modulated growth for fabricating of MOF nanocrystals. Nucleation is controlled and modulated by additives with the same functional groups as the organic linkers to impede the coordination interaction between metal ions and organic linkers. The competition between the additives and the growth species (linkers) leads to selective coordination in one of the coordination modes (illustrated as blue shells) and favors anisotropic growth. b)–d) Coordination-modulated growth of [Cu(ndc)(dabco)$_{0.5}$] monitored ex situ by TEM. Imaging of samples taken after b) 15 min, c) 20 min, and d) 1 h showing the various types of nanocrystals in agreement with (a). Reproduced with permission from Ref. [76].

dabco-copper units. The other growth orientation [100] (see Section 2.3 on the layer-by-layer growth of the same MOF) requires the coordination through ndc-copper. This ndc-copper interaction, which forms the two-dimensional layer of the MOF, was impeded by the presence of acetic acid as the modulator, because both ndc and acetate have the carboxylate functionality. Therefore, the selective coordination-modulation method enhanced the relative crystal growth in the [001] direction. Quite interestingly, the gas-adsorption studies (N_2 and CO_2) of the nanorod-[Cu(ndc)(dabco)$_{0.5}$] material grown under coordination modulation was significantly enhanced compared to that of the usually obtained microcrystalline powder of [Cu(ndc)(dabco)$_{0.5}$]. This difference was attributed to the higher structural defects of the usual material as compared with the coordination-modulated nano-MOF. Nevertheless, direct evidence of coordinated acetic acid groups during crystallization (as indicated in Figure 21 a) or in the nanorods isolated as a powder has not been reported. Even more generally, the fabrication and characterization of well-defined, stable SAMs of organic ligands at a crystal face of a MOF (i.e. "SAMs@MOFs"), has not been documented to date.

Sanchez, Férey, and co-workers employed a similar concept of coordination modulation for the facile synthesis of nanocrystallites of MIL-89 [(X)Fe_3O(muc)$_3$·*n* Solv] (muc = (2*E*,4*E*)-hexa-2,4-dienedicarboxylate = *trans*,*trans*-muconate; X = Cl, F, OH; CH_3COO; Solv = ethanol, methanol, water).[77] Only using the trimeric acetate [(X)Fe_3O-(CH_3CO_2)$_6$(H_2O)$_3$] (X = CH_3COO), instead of iron(III) chloride or nitrate, in combination with muconic acid led to the formation of transparent monolithic gels under an appropriate choice of temperature, concentration, and synthesis time. The competition between a bifunctional carboxylate as a network former and a monofunctional carboxylate acting as a modifier, induces a reduction in the kinetics of the extended crystallization of MIL-89, making the growth of larger crystals harder and thus the control of the particle size at the nanoscale easier, allowing the formation of the gel. Light scattering and TEM studies at early stages of the particle growth (10 min, 60 °C) revealed nano-objects of close to 20–40 nm in diameter. The MIL-89 sols were used for the preparation of homogeneous thin films by dip-coating and the materials were characterized by synchrotron XRD to confirm the identity of the deposited phase. Generally, this approach has also similarities to the colloid chemistry of ZIF-8 (Section 5.1) which also takes advantage of modulated or arrested-growth induced by constituents of the solvothermal mother solution, rather than using special surfactants or other additives.[68] The nano-MOFs have been shown to be very useful as seeds for the solvothermal fabrication of millimeter thick, dense, homogeneous MOF membranes.[78]

6. Atomistic Theoretical Simulations of MOF Surfaces and MOF Growth

From a very early stage, atomistic theoretical simulations contributed substantially to the understanding and development of MOFs and PCPs.[79] This was mainly because well-established methods for the simulation of host–guest interactions for zeolite-type porous materials were already available.[80] In these cases, the experimentally determined structures are used for the calculation and parameterized, classical, molecular mechanics (MM) type potential-energy expressions are employed to describe the host–guest interactions. By a Monte Carlo sampling in the grand canonical ensemble (GCMC), the pressure dependence of the loading of the porous material can be simulated.[81] Interestingly, even non-existent MOF structures, extrapolated from known ones, were investigated to establish tendencies of, for example, hydrogen adsorption.[82] An even more striking example for the relevance of atomistic simulations is the fact that two years before the first experimental results on guest-molecule mobility were reported[83] the first theoretical simulations had been performed.[84]

However, the majority of theoretical investigations focused solely on ideal crystalline systems using 3D periodic boundary conditions, and even the few exceptions, employing non-periodic cluster models, have used systems that mimic the ideal periodic framework. Consequently, only very few computational studies were dedicated to the study of defects and disorder in the network,[85] or unknown framework structures and topologies.[86] From the previous discussion of the available experimental data on SURMOFs it is clear that the most important "defect" is actually the surface itself,

which results from breaking the periodic boundary conditions in one direction. Despite its relevance, this specific situation is currently untouched by theoretical investigations.[87] Also, the closely related aspect of MOF growth occurring at the surface has not yet been addressed by computational studies. Without doubt, an atomically resolved theoretical picture of the structure of a MOF surface, such as the possible acetate-terminated [111] surface of $[Cu_3(btc)_2]$, illustrated in Figure 22, will be of the utmost importance for future

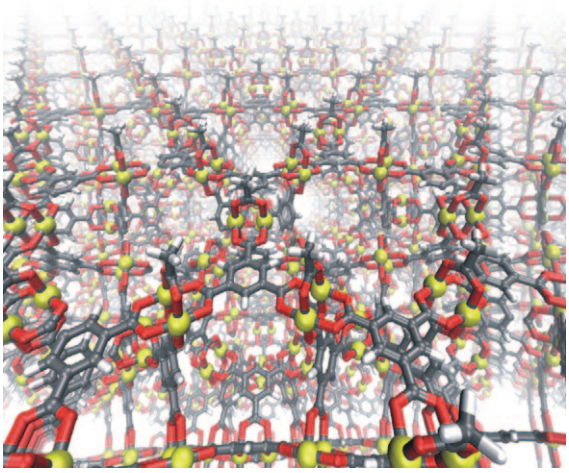

Figure 22. Perspective view on an acetate terminated [111] surface of $[Cu_3(btc)_2]$ computed with a preliminary flexible force field for copper paddlewheel systems.[94]

developments. Such progress would be reminiscent of the situation, when both electronic structure calculations and experimental measurements converged to explain the complex structure exposed at the reconstructed silicon surface, a surface which deviates substantially from the simple bulk structure.[88] In this Section, the first few theoretical attempts to go beyond the ideal crystalline structure will be briefly summarized, however these are still far away from tackling the MOF surface. In this context, the difficulties involved in describing such systems will be commented on, and some conceptual guidelines to be followed in the further development will be named. However, there is currently nothing to Review on the theoretical investigation of MOF surfaces, interfaces, or growth mechanisms, which is clearly a missing piece in the puzzle. The essential ingredient for a theoretical treatment of MOF surfaces, or any kind of structure beyond the ideal crystalline case, is a theoretical model that also accurately includes the intraframework interactions. Quantum mechanics methods, such as periodic density functional theory (DFT) based methods, are in principle, the method of choice, but owing to the size of the systems and the need to sample numerous configurations it is often impossible to use them.[79b] Thus, flexible molecular mechanics methods need to be used, but fully flexible force fields that are able to reproduce the intraframework interactions, especially of the inorganic fragments, are scarce. One of the first such flexible force fields was used by Greathouse and Allendorf to study the interaction of water molecules with IRMOF-1.[89] A collapse of the structure at about 4 wt% of loaded water was observed, in line with the experimental data. In a way, this early work tackles the growth problem indirectly by simulating the reverse process of structural collapse.

The example is also instructive to reveal what is still missing in the simulation that prevents atomistically modeling the IRMOF-1 growth. A simple two-body interaction was used to model the interaction between the metal center and the ligand atom, this model allows for the competition of water with the linker carboxylate groups for the zinc coordination sites. However, the model does not allow for a protonation of the carboxylate groups or of the central oxygen atom of the Zn_4O unit, constraining the system unphysically. Thus, to model the growth of MOFs, either large scale ab initio MD simulations[90] will have to be performed or new and improved molecular mechanics models which allow for reactive bond breaking will have to be developed for MOFs.[91].

Other flexible force fields have been developed (see Ref. [79b] for a discussion). Importantly, the force fields for the MIL-53 type materials[92] are able to explain the "breathing" effect of these systems that occurs with guest-molecule adsorption.[93] Note, that for example, intermediate phases with alternating expanded and contracted pores could be considered as structurally "defect" in the sense of deviating from the experimentally determined ideal crystalline structure. Other flexible molecular mechanics models for the IRMOF series of frameworks were used to determine the atomistic structure in the presence substituted linkers which reduce the symmetry, resulting in a variety of supramolecular isomers.[85] More recently, an accurate first-principle-derived force field for covalent organic frameworks was used to compute strain energies for experimentally unknown topologies.[86] It was also used to model the hydrogen-storage capacity of the as yet unsynthesized COFs.[82] All these results demonstrate that theoretical models are currently developed, which go beyond the constraint of using only experimentally determined framework structures, a necessary condition for modeling MOF surfaces and interfaces. For the theoretical calculation of the surfaces of bulk materials, such as semiconductors or metal oxides, the surface termination is generated by "slicing" the bulk material and relaxing the generated "dangling" (unsaturated) bonds. However, for the hybrid MOF materials, crystallized under solvothermal growth conditions such "dangling" bonds can be clearly ruled out.[87] Most likely the weaker metal–ligand coordination bonds will be broken and the resulting metal coordination sites are saturated, for example, by solvent molecules. As an example, the $[Cu_3(btc)_2]$ surface shown in Figure 22 is assumed to be terminated by acetate molecules, because $[Cu_3(btc)_2]$ can be grown at room temperature in the LbL mode from the preformed acetate paddlewheel SBU $Cu_2(CO_2Et)_4$.[20] In general, solvent molecules will compete with the linkers for metal coordination sites, thus an atomistic picture of a MOF surface will need to include solvation effects. For coordination compounds, these interactions might be different to the purely dispersive and electrostatic interactions (hydrogen bonding) present in organic systems, such as proteins, because coordination bonds could be

involved. Again, the surface structure and growth mechanism are completely entangled problems and improved theoretical models will have to be developed in the future.

7. Conclusion

Over the decades of research on porous coordination polymers, several thousands of compounds have been reported which may, more or less strictly, be classed as PCPs and MOFs. Most of the research was devoted to the synthesis and structural characterization, and to the development of principles or concepts for planning MOF synthesis and understanding the structural features of the products. The key properties of MOFs, namely porosity and tailored coordination space, are intensely investigated within the wide context of host–guest chemistry including gas storage, gas separation, catalysis, drug-release, and bioimaging. Flexible frameworks with responsive properties to external stimuli, including redox activity and possibly electronic and ionic conductivity, represent an emerging class of functional MOFs which hold great promise. All these aspects of PCP and MOF research have been extensively reviewed as summarized in the introduction already.[1–8] The selection of examples collected and selected for this article are quite different in the sense that their focus is not on new MOF compounds or specifically new or modified properties which require synthesis of a new MOF material. Rather, it is intended to present current perspectives on the chemistry of thin films, (nano-)crystals, and surfaces of existing MOF materials. The fabrication of novel functional devices and pushing the limits, ranging from sensing to smart membranes and microreactors will require the fabrication of MOF materials exhibiting the desired properties in a variety of sizes, shapes, and orientations including smooth, nanosized crystalline multilayers and thick, homogeneous, and defect-free films in the micron size regime on the appropriate substrate.[14] The chosen MOF materials need to be available as porous nanocrystals or modules which can be manipulated and positioned into a desired pattern.

As in the case of classic inorganic materials chemistry and technology, crystalline heterostructures of well-defined architectures with abrupt interfaces between the individual domains will add another degree of "design" beyond reticular chemistry and linker functionalization. This area of development is essentially connected with the surface chemistry of MOF crystallites. The transfer of the principles of liquid-phase epitaxial growth of crystals on top of substrate crystals or templates to the field of MOFs represents an important step into this direction and has been shown by the examples of layer-by-layer growth and the hetero- and homoeptiaxial growth of free-standing hybrid crystals of anisotropic and of isotropic MOFs. Nevertheless, almost nothing is known about the details of MOF surface chemistry on the molecular level, either from experiment or theory. In this sense, the in-situ AFM study of the layer-by-layer growth of $[Cu_3(btc)_2]$ may be regarded as a seminal contribution, as are the in-situ studies on $[Cu_3(btc)_2]$ crystallization from real solvothermal solution.

The surface chemistry of MOFs and the chemistry of (nano-) MOFs at surfaces including the characterization of interfaces between different MOFs and the elucidation of the binding properties ("sticking coefficients") of ligands and other functional groups to the different faces of MOF crystallites will become more and more important. Surface reconstruction effects, surface energies, and size- and shape-dependent effects on these parameters need to be investigated. Last but not least, there is a gap between the rapidly developing surface-confined supramolecular coordination chemistry at the gas–solid interface,[95] which includes 2D metal–organic hybrid coordination-polymer structures attached to suitable substrates, and the surface chemistry of MOFs at the liquid–solid interface.

Received: April 25, 2010

[1] a) R. Robson, *Dalton Trans.* **2008**, 5113 – 5131; b) A comprehensive introduction into the MOF field is given in the themed issue *Metal-Organic Frameworks* (Eds.: J. Long, O. M. Yaghi), *Chem. Soc. Rev.* **2009**, *38*, 1201 – 1508.

[2] a) G. Férey, *Struct. Bonding* **2009**, *132*, 87 – 134; b) G. Férey, C. Serre, *Chem. Soc. Rev.* **2009**, *38*, 1380 – 1399; c) G. Férey, *Dalton Trans.* **2009**, 4400 – 4415; d) G. Férey, *Chem. Soc. Rev.* **2008**, *37*, 191 – 214.

[3] a) J. Seo, H. Sakamoto, R. Matsuda, S. Kitagawa, *J. Nanosci. Nanotechnol.* **2010**, *10*, 3 – 20; b) S. Noro, S. Kitagawa, T. Akutagawa, T. Nakamura, *Prog. Polym. Sci.* **2009**, *34*, 240 – 279; c) T. Uemura, N. Yanai, S. Kitagawa, *Chem. Soc. Rev.* **2009**, *38*, 1228 – 1236; d) S. Bureekaew, S. Shimomura, S. Kitagawa, *Sci. Technol. Adv. Mater.* **2008**, *9*, 014108; e) S. Kitagawa, R. Matsuda, *Coord. Chem. Rev.* **2007**, *251*, 2490 – 2509; f) M. Higuchi, S. Horike, S. Kitagawa, *Supramol. Chem.* **2007**, *19*, 75 – 78; g) T. Uemura, S. Horike, S. Kitagawa, *Chem. Asian J.* **2006**, *1*, 36 – 44; h) U. Uemura, R. Matsuda, S. Kitagawa, *J. Solid State Chem.* **2005**, *178*, 2420 – 2429.

[4] a) M. O'Keeffe, M. A. Peskov, S. J. Ramsden, O. M. Yaghi, *Acc. Chem. Res.* **2008**, *41*, 1782 – 1789; b) O. Delgado-Friedrichs, M. O'Keeffe, O. M. Yaghi, *Phys. Chem. Chem. Phys.* **2007**, *9*, 1035 – 1043; c) J. L. C. Rowsell, O. M. Yaghi, *Microporous Mesoporous Mater.* **2004**, *73*, 3 – 14; d) O. M. Yaghi, M. O'Keeffe, N. W. Ockwig, H. K. Chae, M. Eddaoudi, J. Kim, *Nature* **2003**, *423*, 705 – 714.

[5] a) M. Kawano, M. Fujita, *Coord. Chem. Rev.* **2007**, *251*, 2592 – 2605; b) D. Maspoch, D. Ruiz-Molina, J. Veciana, *Chem. Soc. Rev.* **2007**, *36*, 770 – 818; c) A. Y. Robin, K. M. Fromm, *Coord. Chem. Rev.* **2006**, *250*, 2127 – 2157.

[6] a) R. J. Kuppler, D. J. Timmons, Q. R. Fang, J. R. Li, T. A. Makal, M. D. Young, D. Q. Yuan, D. Zhao, W. J. Zhuang, H. C. Zhou, *Coord. Chem. Rev.* **2009**, *253*, 3042 – 3066; b) Y. G. Huang, F. L. Jiang, M. C. Hong, *Coord. Chem. Rev.* **2009**, *253*, 2814 – 2834; c) D. Farrusseng, S. Aguado, C. Pinel, *Angew. Chem.* **2009**, *121*, 7638 – 7649; *Angew. Chem. Int. Ed.* **2009**, *48*, 7502 – 7513; d) A. U. Czaja, N. Trukhan, U. Müller, *Chem. Soc. Rev.* **2009**, *38*, 1284 – 1293; e) J. R. Li, R. J. Kuppler, H. C. Zhou, *Chem. Soc. Rev.* **2009**, *38*, 1477 – 1504; f) S. Q. Ma, *Pure Appl. Chem.* **2009**, *81*, 2235 – 2251; g) L. J. Murray, M. Dinca, J. R. Long, *Chem. Soc. Rev.* **2009**, *38*, 1294 – 1314; h) M. D. Allendorf, C. A. Bauer, R. K. Bhakta, R. J. T. Houk, *Chem. Soc. Rev.* **2009**, *38*, 1330 – 1352; i) C. Z. Mu, F. Xu, W. Lei, *Annu. Rep. Prog. Chem.* **2007**, *19*, 1345 – 1356.

[7] D. J. Tranchemontagne, J. L. Mendoza-Cortes, M. O'Keeffe, O. M. Yaghi, *Chem. Soc. Rev.* **2009**, *38*, 1257 – 1283.

[8] M. O'Keefe, *Chem. Soc. Rev.* **2009**, *38*, 1215 – 1217.

[9] a) F. Di Renzo, F. Fajula, *Zeolites and Ordered Mesoporous Materials: Progress and Prospects* **2005**, *157*, 1 – 12; b) T. Bein, S. Mintova, *Zeolites and Ordered Mesoporous Materials: Progress and Prospects* **2005**, *157*, 263 – 288; c) H. Jiang, B. Q. Zhang, Y. S. Lin, Y. D. Li, *Chin. Sci. Bull.* **2004**, *49*, 2547 – 2554; d) E. E. McLeary, J. C. Jansen, F. Kapteijn, *Microporous Mesoporous Mater.* **2006**, *90*, 198 – 220.

[10] a) A. S. T. Chiang, K. J. Chao, *J. Phys. Chem. Solids* **2001**, *62*, 1899 – 1910; b) L. Tosheva, V. P. Valtchev, *Chem. Mater.* **2005**, *17*, 2494 – 2513.

[11] T. Uemura, S. Kitagawa, *Chem. Lett.* **2005**, *34*, 132 – 137.

[12] A. M. Spokoyny, D. Kim, A. Sumrein, C. A. Mirkin, *Chem. Soc. Rev.* **2009**, *38*, 1218 – 1227.

[13] L. Catala, F. Volatron, D. Brinzei, T. Mallah, *Inorg. Chem.* **2009**, *48*, 3360 – 3370.

[14] D. Zacher, O. Shekhah, C. Wöll, R. A. Fischer, *Chem. Soc. Rev.* **2009**, *38*, 1418 – 1429.

[15] M. Kind, C. Wöll, *Prog. Surf. Sci.* **2009**, *84*, 230 – 278.

[16] a) B. C. Bunker, P. C. Rieke, B. J. Tarasevich, A. A. Campbell, G. E. Fryxell, G. L. Graff, L. Song, J. Liu, J. W. Virden, G. L. McVay, *Science* **1994**, *264*, 48 – 55; b) S. Feng, T. Bein, *Nature* **1994**, *368*, 834 – 836; c) J. Aizenberg, A. J. Black, G. M. Whitesides, *J. Am. Chem. Soc.* **1999**, *121*, 4500 – 4509; d) F. C. Meldrum, J. Flath, W. Knoll, *J. Mater. Chem.* **1999**, *9*, 711 – 723; e) J. W. P. Hsu, Z. R. Tian, N. C. Simmons, C. M. Matzke, J. A. Voigt, J. Liu, *Nano Lett.* **2005**, *5*, 83 – 86; f) J. S. Lee, Y.-J. Lee, E. L. Tae, Y. S. Park, K. B. Yoon, *Science* **2003**, *301*, 818 – 821; g) D. Wang, J. Liu, Q. Huo, Z. Nie, W. Lu, R. E. Williford, Y.-B. Jiang, *J. Am. Chem. Soc.* **2006**, *128*, 13670 – 13671.

[17] S. Hermes, F. Schröder, R. Chelmowski, C. Wöll, R. A. Fischer, *J. Am. Chem. Soc.* **2005**, *127*, 13744.

[18] a) E. Biemmi, C. Scherb, T. Bein, *J. Am. Chem. Soc.* **2007**, *129*, 8054 – 8055; b) E. Biemmi, A. Darga, N. Stock, T. Bein, *Microporous Mesoporous Mater.* **2008**, *114*, 380 – 386.

[19] C. Scherb, A. Schödel, T. Bein, *Angew. Chem.* **2008**, *120*, 5861 – 5863; *Angew. Chem. Int. Ed.* **2008**, *47*, 5777 – 5779.

[20] a) O. Shekhah, H. Wang, S. Kowarik, F. Schreiber, M. Paulus, M. Tolan, C. Sternemann, F. Evers, D. Zacher, R. A. Fischer, C. Wöll, *J. Am. Chem. Soc.* **2007**, *129*, 15118 – 15119; b) C. Munuera, O. Shekhah, H. Wang, C. Wöll, C. Ocal, *Phys. Chem. Chem. Phys.* **2008**, *10*, 7257 – 7261; c) O. Shekhah, H. Wang, D. Zacher, R. A. Fischer, C. Wöll, *Angew. Chem.* **2009**, *121*, 5138 – 5142; *Angew. Chem. Int. Ed.* **2009**, *48*, 5038 – 5041; d) O. Shekhah, H. Wang, T. Strunskus, P. Cyganik, D. Zacher, R. Fischer, C. Wöll, *Langmuir* **2007**, *23*, 7440 – 7442.

[21] a) G. Decher, *Science* **1997**, *277*, 1232 – 1237; b) *Multilayer Thin Films* (Eds.: G. Decher, J. B. Schlenoff), Wiley-VCH, Weinheim, **2003**; c) K. Ariga, J. P. Hill, Q. M. Ji, *Phys. Chem. Chem. Phys.* **2007**, *9*, 2319 – 2340.

[22] a) H. Lee, L. J. Kepley, H. G. Hong, T. E. Mallouk, *J. Am. Chem. Soc.* **1988**, *110*, 618 – 620; b) H. Lee, L. J. Kepley, H. G. Hong, S. Akhter, T. E. Mallouk, *J. Phys. Chem.* **1988**, *92*, 2597 – 2601; c) H. G. Hong, D. D. Sackett, T. E. Mallouk, *Chem. Mater.* **1991**, *3*, 521 – 527; d) H.-N. Kim, S. W. Keller, T. E. Mallouk, J. Schmitt, G. Decher, *Chem. Mater.* **1997**, *9*, 1414 – 1421.

[23] a) H. C. Yang, K. Aoki, H. G. Hong, D. D. Sackett, M. F. Arendt, S. K. Yau, C. M. Bell, T. E. Mallouk, *J. Am. Chem. Soc.* **1993**, *115*, 11855 – 11862; b) C. M. Bell, S. W. Keller, V. M. Lynch, T. E. Mallouk, *Mater. Chem. Phys.* **1993**, *35*, 225 – 232; c) C. M. Bell, M. F. Arendt, L. Gomez, R. H. Schmeh, T. E. Mallouk, *J. Am. Chem. Soc.* **1994**, *116*, 8374 – 8375.

[24] a) S. Cobo, G. Molnar, J. A. Real, A. Bousseksou, *Angew. Chem.* **2006**, *118*, 5918 – 5921; *Angew. Chem. Int. Ed.* **2006**, *45*, 5786 – 5789; b) G. Molnár, S. Cobo, J. A. Real, F. Carcenac, E. Daran, C. Vieu, A. Bousseksou, *Adv. Mater.* **2007**, *19*, 2163 – 2167; c) G. Agustí, R. Ohtani, K. Yoneda, A. B. Gaspar, M. Ohba, J. F. Sanchez-Royo, M. C. Munoz, S. Kitagawa, J. A. Real, *Angew. Chem.* **2009**, *121*, 9106 – 9109; *Angew. Chem. Int. Ed.* **2009**, *48*, 8944 – 8947; d) M. Ohba, K. Yoneda, G. Agustí, M. C. Munoz, A. B. Gaspar, J. A. Real, M. Yamasaki, H. Ando, Y. Nakao, S. Sakaki, S. Kitagawa, *Angew. Chem.* **2009**, *121*, 4861 – 4865; *Angew. Chem. Int. Ed.* **2009**, *48*, 4767 – 4771.

[25] G. Agustí, S. Cobo, A. B. Gaspar, G. Molnar, N. O. Moussa, P. A. Szilagyi, V. Palfi, C. Vieu, M. C. Munoz, J. A. Real, A. Bousseksou, *Chem. Mater.* **2008**, *20*, 6721 – 6732.

[26] a) R. Yerushalmi, A. Scherz, M. E. van der Boom, *J. Am. Chem. Soc.* **2004**, *126*, 2700 – 2701; b) M. Altman, A. D. Shukla, T. Zubkov, G. Evmenenko, P. Dutta, M. E. van der Boom, *J. Am. Chem. Soc.* **2006**, *128*, 7374 – 7382; c) M. Altman, O. Zenkina, G. Evmenenko, P. Dutta, M. E. van der Boom, *J. Am. Chem. Soc.* **2008**, *130*, 5040 – 5041; d) L. Motiei, M. Altman, T. Gupta, F. Lupo, A. Gulino, G. Evmenenko, P. Dutta, M. E. van der Boom, *J. Am. Chem. Soc.* **2008**, *130*, 8913 – 8915.

[27] a) J. E. Wong, W. Richtering, *Curr. Opin. Colloid Interface Sci.* **2008**, *13*, 403 – 412; b) J. J. Cerdà, B. F. Qiao, C. Holm, *Soft Matter* **2009**, *5*, 4412 – 4425; c) C. Li, J. Zhang, S. Yang, B. L. Li, Y. Y. Li, X. Z. Zhang, R. X. Zhuo, *Phys. Chem. Chem. Phys.* **2009**, *11*, 8835 – 8840; d) K. C. Wood, H. F. Chuang, R. D. Batten, D. M. Lynn, P. T. Hammond, *Proc. Natl. Acad. Sci. USA* **2006**, *103*, 10207 – 10212.

[28] a) S. S. Y. Chui, S. M. F. Lo, J. P. H. Charmant, A. G. Orpen, I. D. Williams, *Science* **1999**, *283*, 1148 – 1150; b) U. Müller, M. Schubert, F. Teich, H. Puetter, K. Schierle-Arndt, J. Pastre, *J. Mater. Chem.* **2006**, *16*, 626 – 636; c) B. Xiao, P. S. Wheatley, X. B. Zhao, A. J. Fletcher, S. Fox, A. G. Rossi, I. L Megson, S. Bordiga, L. Regli, K. M. Thomas, R. E. Morris, *J. Am. Chem. Soc.* **2007**, *129*, 1203 – 1209.

[29] a) G. Férey, *J. Solid State Chem.* **2000**, *152*, 37 – 48; b) F. Taulelle, *Curr. Opin. Solid State Mater. Sci.* **2001**, *5*, 397 – 405; c) G. Férey, C. Mellot-Draznieks, C. Serre, F. Millange, J. Dutour, S. Surble, I. Margiolaki, *Science* **2005**, *309*, 2040 – 2042; d) A. Ramanan, M. S. Whittingham, *Cryst. Growth Des.* **2006**, *6*, 2419 – 2421.

[30] a) K. Seki, W. Mori, *J. Phys. Chem. B* **2002**, *106*, 1380 – 1385; b) R. Kitaura, F. Iwahori, R. Matsuda, S. Kitagawa, Y. Kubota, M. Takata, T. C. Kobayashi, *Inorg. Chem.* **2004**, *43*, 6522 – 6524; c) H. Chun, D. N. Dybtsev, H. Kim, K. Kim, *Chem. Eur. J.* **2005**, *11*, 3521 – 3529; d) D. Tanaka, S. Horike, S. Kitagawa, M. Ohba, M. Hasegawa, Y. Ozawa, K. Toriumi, *Chem. Commun.* **2007**, 3142 – 3144; e) T. Uemura, Y. Ono, K. Kitagawa, S. Kitagawa, *Macromolecules* **2008**, *41*, 87 – 94; f) D. Tanaka, M. Higuchi, S. Horike, R. Matsuda, Y. Kinoshita, N. Yanai, S. Kitagawa, *Chem. Asian J.* **2008**, *3*, 1343 – 1349.

[31] O. Shekhah, H. Wang, M. Paradinas, C. Ocal, B. Schupbach, A. Terfort, D. Zacher, R. A. Fischer, C. Wöll, *Nat. Mater.* **2009**, *8*, 481 – 484.

[32] a) O. M. Yaghi, *Nat. Mater.* **2007**, *6*, 92 – 93; b) R. Q. Snurr, J. T. Hupp, S. T. Nguyen, *AIChE J.* **2004**, *50*, 1090 – 1095; c) S. R. Batten, R. Robson, *Angew. Chem.* **1998**, *110*, 1558 – 1595; *Angew. Chem. Int. Ed.* **1998**, *37*, 1460 – 1494.

[33] M. Eddaoudi, D. B. Moler, H. Li, B. Chen, T. M. Reineke, M. O'Keeffe, O. M. Yaghi, *Acc. Chem. Res.* **2001**, *34*, 319 – 330.

[34] M. Eddaoudi, J. Kim, N. Rosi, D. Vodak, J. Wachter, M. O'Keeffe, O. M. Yaghi, *Science* **2002**, *295*, 469 – 472.

[35] D. J. Tranchemontagne, J. R. Hunt, O. M. Yaghi, *Tetrahedron* **2008**, *64*, 8553 – 8557.

[36] J. Hafizovic, M. Bjørgen, U. Olsbye, P. D. C. Dietzel, S. Bordiga, C. Prestipino, C. Lamberti, K. P. Lillerud, *J. Am. Chem. Soc.* **2007**, *129*, 3612 – 3620.

[37] B.-Q. Ma, K.-L. Mulfort, J. T. Hupp, *Inorg. Chem.* **2005**, *44*, 4912 – 4914.

[38] a) D. Zacher, K. Yusenko, A. Bétard, M. Meilikhov, T. Ladnorg, O. Shekhah, A. Terfort, C. Wöll, R. A. Fischer, *Chem. Eur. J.* **2011**, DOI: 10.1002/chem.201002381; b) K. Kanaizuka, R.

Haruki, O. Sakata, M. Yoshimoto, Y. Akita, H. Kitagawa, *J. Am. Chem. Soc.* **2008**, *130*, 15778 – 15779.
[39] M. D. Allendorf, R. J. T. Houk, L. Andruszkiewicz, A. A. Talin, J. Pikarsky, A. Choudhury, K. A. Gall, P. J. Hesketh, *J. Am. Chem. Soc.* **2008**, *130*, 14404 – 14405.
[40] O. Zybaylo, O. Shekhah, R. Schmit, C. Wöll, *Phys. Chem. Chem. Phys.* **2010**, DOI: 10.1039/b927601g.
[41] F. Schüth, *Curr. Opin. Solid. State Mater. Sci.* **2001**, *5*, 389 – 395.
[42] R. E. Morris, *ChemPhysChem* **2009**, *10*, 327 – 329.
[43] F. Millange, M. I. Medina, N. Guillou, G. Férey, K. M. Golden, R. I. Walton, *Angew. Chem.* **2010**, *122*, 775 – 778; *Angew. Chem. Int. Ed.* **2010**, *49*, 763 – 766.
[44] S. Surblé, F. Milange, C. Serre, G. Férey, R. J. Walton, *Chem. Commun.* **2006**, 1518 – 1520.
[45] C. S. Cundy, P. A. Cox, *Microporous Mesoporous Mater.* **2005**, *82*, 1 – 78.
[46] J. A. Rood, W. C. Boggess, B. C. Noll, K. W. Henderson, *J. Am. Chem. Soc.* **2007**, *129*, 13675 – 13682.
[47] a) M. W. Anderson, L. I. Meza, J. R. Agger, M. P. Attfield, M. Shöâeè, C. B. Chong, A. Umemura, C. S. Cundy, *Mater. Surf. Sci.* **2008**, 95 – 122; b) R. Brent, M. W. Anderson, *Angew. Chem.* **2008**, *120*, 5407 – 5410; *Angew. Chem. Int. Ed.* **2008**, *47*, 5327 – 5330; c) M. B. Roeffaers, R. Ameloot, M. Baruah, H. Uji-i, M. Bulut, G. De Cremer, U. Müller, P. A. Jacobs, J. Hofkens, B. F. Sels, D. E. De Vos, *J. Am. Chem. Soc.* **2008**, *130*, 5763 – 5772; d) M. W. Anderson, J. R. Agger, L. I. Meza, C. B. Chong, C. S. Cundy, *Faraday Discuss.* **2007**, *136*, 143 – 156; e) L. I. Meza, M. W. Anderson, J. R. Agger, *Chem. Commun.* **2007**, 2473 – 2475; f) J. R. Agger, N. Hanif, N. C. S. Cundy, A. P. Wade, S. Dennison, P. A. Rawlinson, M. W. Anderson, *J. Am. Chem. Soc.* **2003**, *125*, 830 – 839; g) P. Q. Miraglia, B. Yilmaz, J. Warzywoda, S. Bazzana, A. Sacco, *Microporous Mesoporous Mater.* **2004**, *69*, 71 – 76; h) S. Yamamoto, S. Sugiyama, O. Matsuoka, K. Kohmura, T. Honda, Y. Banno, H. Nozoye, *J. Phys. Chem.* **1996**, *100*, 18474 – 18482.
[48] K. Szelagowska-Kunstman, P. Cyganik, M. Goryl, D. Zacher, Z. Puterova, R. A. Fischer, M. Szymonski, *J. Am. Chem. Soc.* **2008**, *130*, 14446 – 14447.
[49] M. Shöâeé, J. R. Agger, M. W. Anderson, M. P. Attfield, *CrystEngComm* **2008**, *10*, 646 – 648.
[50] a) N. S. John, C. Scherb, M. Shöâeé, M. W. Anderson, M. P. Attfield, T. Bein, *Chem. Commun.* **2009**, 6294 – 6296; b) M. Shöâeé, M. W. Anderson, M. P. Attfield, *Angew. Chem.* **2008**, *120*, 8653 – 8656; *Angew. Chem. Int. Ed.* **2008**, *47*, 8525 – 8528.
[51] I. V. Markov, *Crystal Growth for Beginners: Fundamentals of Nucleation, Crystal Growth and Epitaxy*, 2nd ed. World Scientific, Singapore, **2003**.
[52] a) *Chemical Vapour Deposition: Precursors, Processes and Applications* (Eds.: A. Jones, M. Hitchman), RSC Publishing, London, **2009**; b) M. Leskelä, M. Ritala, *Angew. Chem.* **2003**, *115*, 5706 – 5713; *Angew. Chem. Int. Ed.* **2003**, *42*, 5548 – 5554.
[53] a) J. C. MacDonald, P. C. Dorrestein, M. M. Pilley, M. M. Foote, J. L. Lundburg, R. W. Henning, A. J. Schultz, J. L. Manson, *J. Am. Chem. Soc.* **2000**, *122*, 11692 – 11702; b) T.-J. Luo, J. C. MacDonald, G. T. R. Palmore, *Chem. Mater.* **2004**, *16*, 4916 – 4927.
[54] J. C. Noveron, M. S. Lah, R. E. Del Sesto, A. M. Arif, J. S. Miller, P. J. Stang, *J. Am. Chem. Soc.* **2002**, *124*, 6613 – 6625.
[55] a) S. Ferlay, W. Hosseini, *Chem. Commun.* **2004**, 788 – 789; b) P. Dechambenoit, S. Ferlay, M. W. Hosseini, *Cryst. Growth Des.* **2005**, *5*, 2310 – 2312; c) E. F. Brès, S. Ferlay, P. Dechambenoit, H. Leroux, M. W. Hosseini, S. Reyntjens, *J. Mater. Chem.* **2007**, *17*, 1559 – 1562; d) P. Dechambenoit, S. Ferlay, N. Kyritsakas, M. W. Hosseini, *J. Am. Chem. Soc.* **2008**, *130*, 17106 – 17113; e) P. Dechambenoit, S. Ferlay, N. Kyritsakas, M. W. Hosseini, *Chem. Commun.* **2009**, 1559 – 1561; f) B. K. Olmsted, S. Ferlay, P. Dechambenoit, M. W. Hosseini, M. D. Ward, *Cryst. Growth Des.* **2009**, *9*, 2841 – 2847; g) P. Dechambenoit, S. Ferlay, N. Kyritsakas, M. W. Hosseini, *Chem. Commun.* **2010**, *46*, 868 – 870.
[56] S. Furukawa, K. Hirai, K. Nakagawa, Y. Takashima, R. Matsuda, T. Tsuruoka, M. Kondo, R. Haruki, D. Tanaka, H. Sakamoto, S. Shimomura, O. Sakata, S. Kitagawa, *Angew. Chem.* **2009**, *121*, 1798 – 1802; *Angew. Chem. Int. Ed.* **2009**, *48*, 1766 – 1770.
[57] S. Furukawa, K. Hirai, Y. Takashima, K. Nakagawa, M. Kondo, T. Tsuruoka, O. Sakata, S. Kitagawa, *Chem. Commun.* **2009**, 5097 – 5099.
[58] K. Koh, A. G. Wong-Foy, A. J. Matzger, *Chem. Commun.* **2009**, 6162 – 6164.
[59] Y.-S. Yoo, H.-K. Jeong, *Cryst. Growth Des.* **2010**, *10*, 1283 – 1288.
[60] a) H. Li, M. Eddaoudi, M. O'Keeffe, O. M. Yaghi, *Nature* **1999**, *402*, 276 – 279; b) M. Eddaoudi, J. Kim, N. Rosi, D. Vodak, J. Wachter, M. O'Keeffe, O. M. Yaghi, *Science* **2002**, *295*, 469 – 472.
[61] a) H. Deng, C. J. Doonan, H. Furukawa, R. B. Ferreira, J. Towne, C. B. Knobler, B. Wang, O. M. Yaghi, *Science* **2010**, *327*, 846 – 850; b) K. Koh, A. G. Wong-Foy, A. J. Matzger, *Angew. Chem.* **2008**, *120*, 689 – 692; *Angew. Chem. Int. Ed.* **2008**, *47*, 677 – 680; c) K. Koh, A. G. Wong-Foy, A. J. Matzger, *J. Am. Chem. Soc.* **2009**, *131*, 4184 – 4185.
[62] A. C. McKinlay, R. E. Morris, P. Horcajada, G. Férey, R. Gref, P. Couvreur, C. Serre, *Angew. Chem.* **2010**, *122*, 6400 – 6406.
[63] a) P. Horcajada, T. Chalati, C. Serre, B. Gillet, C. Sebrie, T. Baati, J. F. Eubank, D. Heurtaux, P. Clayette, C. Kreuz, J.-S. Chang, Y. K. Hwang, V. Marsaud, P.-N. Bories, L. Cynober, S. Gil, G. Férey, P. Couvreur, R. Gref, *Nat. Mater.* **2010**, *9*, 172 – 178; b) P. Horcajada, C. Serre, M. Vallet-Regí, M. Sebban, F. Taulelle, G. Férey, *Angew. Chem.* **2006**, *118*, 6120 – 6124; *Angew. Chem. Int. Ed.* **2006**, *45*, 5974 – 5978; c) P. Horcajada, C. Serre, G. Maurin, N. A. Ramsahye, F. Balas, M. Vallet-Regí, M. Sebban, F. Taulelle, G. Férey, *J. Am. Chem. Soc.* **2008**, *130*, 6774 – 6780.
[64] a) N. J. Hinks, A. C. McKinlay, B. Xiao, P. S. Wheatley, R. E. Morris, *Microporous Mesoporous Mater.* **2010**, *129*, 330 – 334; b) B. Xiao, P. J. Byrne, P. S. Wheatley, D. S. Wragg, X. Zhao, A. J. Fletcher, K. M. Thomas, L. Peters, J. S. O. Evans, J. E. Warren, W. Zhou, R. E. Morris, *Nat. Chem.* **2009**, *1*, 289 – 294.
[65] a) W. J. Rieter, K. M. L. Taylor, H. An, W. Lin, W. Lin, *J. Am. Chem. Soc.* **2006**, *128*, 9024 – 9025; b) W. J. Rieter, K. M. L. Taylor, W. Lin, *J. Am. Chem. Soc.* **2007**, *129*, 9852 – 9853; c) K. M. L. Taylor, A. Jin, W. Lin, *Angew. Chem.* **2008**, *120*, 7836 – 7839; *Angew. Chem. Int. Ed.* **2008**, *47*, 7722 – 7725; d) K. M. L. Taylor, W. J. Rieter, W. Lin, *J. Am. Chem. Soc.* **2008**, *130*, 14358 – 14359; e) W. J. Rieter, K. M. Pott, K. M. L. Taylor, W. Lin, *J. Am. Chem. Soc.* **2008**, *130*, 11584 – 11585.
[66] a) Z. Ni, R. I. Masel, *J. Am. Chem. Soc.* **2006**, *128*, 12394; b) S. H. Jhung, J.-H. Lee, J. W. Yoon, C. Serre, G. Férey, J. S. Chang, *Adv. Mater.* **2007**, *19*, 121 – 124.
[67] L.-G. Qiu, Z.-Q. Li, Y. Wu, W. Wang, T. Xu, X. Jiang, *Chem. Commun.* **2008**, 3642 – 3644.
[68] J. Cravillon, S. Munzer, S. J. Lohmeier, A. Feldhoff, K. Huber, M. Wiebcke, *Chem. Mater.* **2009**, *21*, 1410 – 1412.
[69] a) X.-C. Huang, Y.-Y. Lin, J.-P. Zhang, X.-M. Chen, *Angew. Chem.* **2006**, *118*, 1587 – 1589; *Angew. Chem. Int. Ed.* **2006**, *45*, 1557 – 1559; b) K. S. Park, Z. Ni, A. P. Cote, J. Y. Choi, R. Huang, F. J. Uribe-Romo, H. K. Chae, M. O'Keeffe, O. M. Yaghi, *Proc. Natl. Acad. Sci. USA* **2006**, *103*, 10186 – 10191.
[70] D. Zacher, J. Liu, K. Huber, R. A. Fischer, *Chem. Commun.* **2009**, 1031 – 1033.
[71] a) J. Munn, P. Barnes, D. Hausermann, S. A. Axon, J. Klinowski, *Phase Transitions* **1992**, *39*, 129 – 134; b) R. J. Francis, S. J. Price, J. S. O. Evans, S. O'Brien, D. O'Hare, S. M. Clark, *Chem. Mater.* **1996**, *8*, 2102 – 2108; c) R. I. Walton, T. Loiseau, D. O'Hare, G. Férey, *Chem. Mater.* **1999**, *11*, 3201 – 3209; d) R. I. Walton, F. Millange, D. O'Hare, A. T. Davies, G. Sankar, C. R. A. Catlow, *J. Phys. Chem. B* **2001**, *105*, 83 – 90; e) R. Kiebach, N. Pienack, M. E. Ordolff, F. Studt, W. Bensch, *Chem. Mater.* **2006**, *18*, 1196 –

1205; f) G. Sankar, T. Okubo, W. Fan, F. Meneau, *Faraday Discuss.* **2007**, *136*, 157 – 166.
[72] S. Hermes, T. Witte, T. Hikov, D. Zacher, S. Bahnmueller, G. Langstein, K. Huber, R. A. Fischer, *J. Am. Chem. Soc.* **2007**, *129*, 5324 – 5325.
[73] a) L. Rayleigh, *Proc. R. Soc. London Ser. A* **1914**, *90*, 219 – 225; b) P. Mittelbach, G. Porod, *Acta Phys. Austriaca* **1961**, *14*, 185 – 211.
[74] T. Trindade, P. O'Brien, N. L. Pickett, *Chem. Mater.* **2001**, *13*, 3843 – 3858.
[75] W. Clegg, D. R. Harbron, C. D. Homan, P. A. Hunt, I. R. Little, B. P. Straughan, *Inorg. Chim. Acta* **1991**, *186*, 51 – 60.
[76] T. Tsuruoka, S. Furukawa, Y. Takashima, K. Yoshida, S. Isoda, S. Kitagawa, *Angew. Chem.* **2009**, *121*, 4833 – 4837; *Angew. Chem. Int. Ed.* **2009**, *48*, 4739 – 4743.
[77] P. Horcajada, C. Serre, D. Grosso, C. Boissière, S. Perruchas, C. Sanchez, G Férey, *Adv. Mater.* **2009**, *21*, 1931 – 1935.
[78] H. Bux, F. Liang, Y. Li, J. Cravillon, M. Wiebcke, J. Caro, *J. Am. Chem. Soc.* **2009**, *131*, 16000 – 16001.
[79] a) S. Keskin, J. Liu, R. B. Rankin, J. K. Johnson, D. S. Sholl, *Ind. Eng. Chem. Res.* **2009**, *48*, 2355 – 2371; b) M. Tafipolsky, S. Amirjalayer, R. Schmid, *Microporous Mesoporous Mater.* **2010**, *129*, 304 – 318.
[80] P. Demontis, G. B. Suffritti, *Chem. Rev.* **1997**, *97*, 2845 – 2878.
[81] T. Düren, Y.-S. Bae, R. Q. Snurr, *Chem. Soc. Rev.* **2009**, *38*, 1237 – 1247.
[82] a) T. Düren, L. Sarkisov, O. M. Yaghi, R. Q. Snurr, *Langmuir* **2004**, *20*, 2683 – 2689; b) E. Klontzas, E. Tylianakis, G. E. Froudakis, *Nano Lett.* **2010**, *10*, 452 – 454.
[83] F. Stallmach, S. Gröger, V. Künzel, J. Kärger, O. M. Yaghi, M. Hesse, U. Müller, *Angew. Chem.* **2006**, *118*, 2177 – 2181; *Angew. Chem. Int. Ed.* **2006**, *45*, 2123 – 2126.
[84] a) L. Sarkisov, T. Düren, R. Q. Snurr, *Mol. Phys.* **2004**, *102*, 211 – 221; b) A. I. Skoulidas, *J. Am. Chem. Soc.* **2004**, *126*, 1356 – 1357.
[85] a) Y. H. Jhon, M. Cho, H. R. Jeon, I. Park, R. Chang, J. L. C. Rowsell, J. Kim, *J. Phys. Chem. C* **2007**, *111*, 16618 – 16625; b) S. Amirjalayer, R. Schmid, *J. Phys. Chem. C* **2008**, *112*, 14980 – 14987.
[86] R. Schmid, M. Tafipolsky, *J. Am. Chem. Soc.* **2008**, *130*, 12600 – 12601.
[87] In a recent work the theoretical calculation of a MOF-5 surface was attempted, using a quantum-mechanical method and a slab model. However, the surface was generated by slicing through the strong C_{carb}–C_{ph} bond, leading to a physically unreasonable termination: K. Odbadrakh, J. P. Lewis, D. M. Nicholson, T. Petrova, A. Michalkova, J. Leszczynski, *J. Chem. Phys. C* **2010**, *114*, 3732 – 3736.
[88] a) H. J. Freund, H. Kuhlenbeck, V. Staemmler, *Rep. Prog. Phys.* **1996**, *59*, 283 – 347; b) C. B. Duke, *Chem. Rev.* **1996**, *96*, 1237 – 1259.
[89] J. A. Greathouse, M. D. Allendorf, *J. Am. Chem. Soc.* **2006**, *128*, 10678 – 10679.
[90] a) C. Tuma, J. Sauer, *Angew. Chem.* **2005**, *117*, 4847 – 4849; *Angew. Chem. Int. Ed.* **2005**, *44*, 4769 – 4771; b) J. Hafner, L. Benco, T. Bucko, *Top. Catal.* **2006**, *37*, 41 – 54.
[91] A. C. T. van Duin, S. Dasgupta, F. Lorant, W. A. Goddard, *J. Phys. Chem. A* **2001**, *105*, 9396 – 9409.
[92] C. Serre, F. Millange, C. Thouvenot, M. Nogues, G. Marsolier, D. Louer, G. Férey, *J. Am. Chem. Soc.* **2002**, *124*, 13519 – 13526.
[93] a) P. L. Llewellyn, G. Maurin, T. Devic, S. Loera-Serna, N. Rosenbach, C. Serre, S. Bourrelly, P. Horcajada, Y. Filinchuk, G. Férey, *J. Am. Chem. Soc.* **2008**, *130*, 12808 – 12814; b) F. Salles, A. Ghoufi, G. Maurin, R. G. Bell, C. Mellot-Draznieks, G. Férey, *Angew. Chem.* **2008**, *120*, 8615 – 8619; *Angew. Chem. Int. Ed.* **2008**, *47*, 8487 – 8491.
[94] S. Amirjalayer, M. Tafipolsky, R. Schmid, unpublished results.
[95] J. V. Barth, *Surf. Sci.* **2009**, *603*, 1533 – 1541.

